Assessing Improved Price Zones in Europe: Flow-Based Market Coupling in Central Western Europe in Focus

Tim Felling,[a] Björn Felten,[a] Paul Osinski,[a] and Christoph Weber[a]*

ABSTRACT

Theoretical papers have identified several sources of inefficiencies of flow-based market coupling (FBMC), the implicit congestion management method used to couple the Central Western European (CWE) electricity markets. These inefficiencies ultimately lead to welfare losses. In this paper, a large-scale model framework is introduced for FBMC assessments, focusing on modeling the capacity allocation and market clearing processes. The present paper completes this framework by presenting a newly developed redispatch model. Furthermore, we provide a case study assessing improved price zone configurations (PZCs) for the CWE electricity system, motivated by the debate on the currently-existing PZC. Our results show that improved PZCs—even while maintaining the number of price zones—can significantly reduce redispatch quantities and overall system costs. Moreover, making use of the insights of (Felten et al., 2021), we explain why increasing the number of price zones may not always increase welfare when using FBMC.

Keywords: Price zones, Zonal pricing, Flow-based market coupling, Electricity market design, Welfare analysis, Redispatch

https://doi.org/10.5547/01956574.44.6.tfel

1. INTRODUCTION

With increasing amounts of variable non-dispatchable electricity generation from renewable sources, the locations of supply and demand of electricity frequently fall apart. Therefore, electricity transmission and congestion management become more and more important for power systems. Their relevance becomes obvious when considering currently observed redispatch amounts and costs in Germany. Both of these quantities have increased by more than 400 % over the last few years (BDEW, 2017). Most of these redispatch measures are taken to avoid overloads of intra-zonal transmission lines (cf. BNetzA and Bundeskartellamt, 2018).

One possible way to cope with the challenge of congestion management can be the implementation of a nodal pricing regime (Hogan, 1992) as applied e.g. in parts of North America or New Zealand (Biggar and Hesamzadeh, 2014). This option is known to yield welfare-optimal market outcomes. However, for various reasons, the European target model builds on coupled yet zonally organized electricity markets. Hence, a transition to nodal pricing would constitute a fundamental

a House of Energy Markets and Finance, University of Duisburg-Essen.

* Corresponding author. House of Energy Markets and Finance, University of Duisburg-Essen. Send correspondence to Chair for Management Science and Energy Economics, Universität Duisburg-Essen, Campus Essen, Fakultät für Wirtschaftswissenschaften, Universitätsstraße 12, 45141 Essen. E-mail: paul.osinski@uni-due.de.

paradigm change and is not likely to occur anytime soon. Thus, alternative price zone configurations (PZCs),[1] which are geared to frequently congested lines, are one option to reduce intra-zonal congestion while maintaining a zonal market design. In the current PZC, price zones are (mostly) aligned with national borders. However, this PZC has eventually been questioned (ACER, 2014; Löschel et al., 2013), and the European Commission has eventually called for a first review of this PZC (European Commission, 2015). Yet, the results of this review process could not be used for a solid and comprehensive assessment of PZCs (Entso-E, 2018a) for various reasons (Felten et al., 2021). To that end, a second bidding zone review has been launched (ACER, 2020). The paper at hand constitutes a contribution into the same direction. Its main research question is how improved PZCs can contribute to enhancements in congestion management. This question is investigated with special regard to FBMC, as this is the applied MC method in Central Western Europe (CWE).

In (Felten et al., 2021), the authors demonstrate that managing congestion of intra-zonal lines is especially ineffective in FBMC-style zonal market designs. Moreover, they work out several reasons for inefficiencies, i.e. welfare losses:

1. In essence, the FBMC process reduces the degrees of freedom of the electricity market clearing problem (EMCP). For this purpose, it uses approximations like the so-called generation shift keys (GSKs) and the base case. In order to compensate for inaccuracies, in conjuction with uncertainties, flow reliability margins (FRMs) are used. All in all, this reduces the feasible region of the EMCP. If the welfare-optimal point is infeasible in the zonal EMCP, the result is a reduction of welfare. The current TSO practice regarding redispatch implies that redispatch will not be used to reach any such point that is infeasible in the EMCP yet feasible in a nodal approach.
2. In Felten et al. (2021) we further explain that the restrictions of the zonal EMCP can also be "too loose". This fact is especially associated with intra-zonal line constraints but also with the aforementioned approximations. We pose the question whether the potentially resulting redispatch can establish a welfare-optimal result.[2]

In practice, inefficiencies of redispatch may moreover result from a tendency of TSOs to minimize quantities (as opposed to costs) in the redispatch process. Also additional start-up costs, opportunity costs (e.g. for the cogeneration of heat) and other factors (e.g. lack of accurate information) may lead to suboptimal TSO decisions. In the paper at hand, we provide a case study that addresses these inefficiencies. A frequently discussed option to improve the efficiency of market coupling in CWE is the re-classification of intra-zonal lines into inter-zonal lines. We investigate the resulting improved price zone configurations (PZCs) and assess the effects in terms of welfare for almost the entire European continent.

To be able to perform such a case study, we present a large-scale model framework that is capable of reproducing all stages of the MC process to a high level of detail; starting with the processes of capacity allocation, proceeding with the clearing of the European day-ahead and intraday markets, and finishing with potentially necessary redispatch measures. The high level of accuracy is achieved by three types of activities: (i) resorting to proven large-scale program tools specialized in grid and market modeling, namely MATPOWER (Zimmermann et al., 2011) and the WILMAR or Joint Market Model (JMM) (Meibom et al., 2006; Weber et al., 2009) incl. its CHP tool (Felten,

1. A list of abbreviations and symbols is given in Appendix A.

2. Note that, within the framework of the so-called "Clean Energy Package", the EU even aims at fostering trade between these coupled price zones by introducing fixed minimum thresholds on inter-zonal lines to be made available for the cross-zonal trade. However, this adjusted regulation does not change the conclusions in (Felten et al., 2021).

2020), (ii) developing program enhancements allowing to model all abovementioned FBMC stages and (iii) implementing tailored data handling routines in order to use consistent input data at different levels of aggregation and to hand over all necessary data between the program stages. With regard to MC procedures, special attention is paid to the fact that, throughout Europe, different methods of MC coexist. In particular, the NTC-based MC is still in use outside of CWE and, thus, it is an important feature of our model to be capable of replicating both MC mechanisms in a combined manner.[3] In addition to model developments related to FBMC, for a comprehensive view on MC efficiency, redispatch must be taken into account. Therefore, a capacious redispatch tool has been developed.

The contributions of the paper at hand are revealed by a review of extant literature. For this purpose, we cluster the existing publications assessing zonal market designs into three groups:

1. The first group analyzes stylized (or rather small-scale) zonal systems. Frequently, the benchmark is the nodal market design as first-best solution (e.g. Ehrenmann and Smeers, 2005; Bjørndal and Jörnsten, 2001, 2007; Oggioni and Smeers, 2013; Grimm et al., 2016a, 2019). Some of these studies (Ehrenmann and Smeers, 2005; Bjørndal and Jörnsten, 2001, 2007; Oggioni and Smeers, 2013) also assume or determine alternative PZCs for their stylized examples. While the use of these stylized examples is a powerful means for understanding/analyzing cause-and-effect relations of MC processes, their value for the quantification of absolute effects, such as welfare changes in real-world systems, is limited (Felten et al., 2021).
2. For this purpose, the second stream of papers encompasses application studies by means of large-scale electricity models. E.g. Neuhoff et al. (2013); Bertsch et al. (2016); Egerer et al. (2015); Trepper et al. (2015); Finck et al. (2018); Marjanovic et al. (2018); Wyrwoll et al. (2018) apply more sophisticated models for the assessment of the existing PZC. A higher level of sophistication can be attained by replicating market processes in more detail, increasing the regional scope, improving granularity of data, enhancing the representation of technical constraints or other measures. For instance, Neuhoff et al. (2013); Bertsch et al. (2016); Egerer et al. (2015) contain detailed representations of the grid. In addition, Bertsch et al. (2016) include transmission grid expansion planning. The market model of Trepper et al. (2015) contains intertemporal constraints (minimum operation times, minimum downtimes, water reservoir filling levels, etc.) and a combined modeling of heat and power sectors and of other technical restrictions. However, Trepper et al. (2015) only use a simplified representation of the grid. These studies are usually based on the existing PZC. E.g. Egerer et al. (2015) and Trepper et al. (2015) assess the effects of splitting the existing German-Austrian price zone whereas Neuhoff et al. (2013) and Bertsch et al. (2016) model the existing PZC and contrast the resulting market outcomes with those of a nodal market design.[4] In contrast to the previously named studies, FBMC procedures are considered in recent works of Finck et al. (2018); Marjanovic et al. (2018); Wyrwoll et al. (2018); Schönheit et al. (2020); Lang et al. (2020); Matthes et al. (2019). Therein, Marjanovic et al. (2018); Finck et al. (2018); Lang et al. (2020) investigate the effects of extending the FBMC region to Central Eastern Europe, while Wyrwoll et al. (2018); Schönheit et al. (2020) present effects of different FBMC parametrizations on trading volumes and Matthes et al. (2019) assess

3. The term "NTC-based" refers to net transfer capacities, which limit bilateral (i.e. zone-to-zone) exchanges.

4. Despite having assigned these studies to the group of large-scale applications, it should be noted that some of these studies only assess a limited set of hours or do not consider important technical constraints.

the effects on market clearing results. Notably, none of these FBMC-focused studies investigates improved PZCs. In turn, the large-scale model framework presented within this paper considers FBMC as well and, at the same time, is applied to assess improved PZCs.[5] Thus, we do not limit the assessment to the existing PZC (or a breakdown of it) and thereby contribute significantly to the above mentioned European Commission request for a more efficient PZC (European Commission, 2015).

3. The third stream of papers departs from basing assessments on the existing PZC (e.g. Burstedde, 2012; Breuer, 2014; Felling and Weber, 2018; Imran et al., 2008; Van den Bergh et al., 2016; Sarfati et al., 2015; Kłos et al., 2014). They address the question of how to determine new price zones, what we henceforth refer to as long-term price zone reconfiguration process. Therein, the focus is often laid on defining a set of criteria or developing an algorithm for grouping nodes to zones. These algorithms use information at the level of (aggregated) grid nodes/transmission lines, i.e. locational marginal prices (LMPs) in Burstedde (2012); Imran et al. (2008); Breuer (2014); Felling and Weber (2018) or power transfer distribution factors (PTDFs) (Sarfati et al., 2015; Kłos et al., 2014; Van den Bergh et al., 2016). Some works also propose highly non-linear or multi-level optimization problems of how to assess optimal price zones in terms of overall welfare (Felling, 2019; Grimm et al., 2019; Ambrosius et al., 2020; Bjørndal and Jörnsten, 2001). Usually, applied models either comprise a detailed grid and a simplified market model or vice versa, i.e. the optimization problems are either solved for reduced data sets with a limited number of zones and hours (Ambrosius et al., 2020), using a heuristic approach (Felling, 2019) or remain unsolved (Bjørndal and Jörnsten, 2001). In all of the mentioned works, real-world complexities are simplified in either one dimension. The paper at hand does not make such compromise when it comes to electricity market modelling. Making use of specialized and proven tools, enhancing them and combining them in the developed model framework allows us to reproduce all stages of the MC process (i.e. capacity allocation, market clearing and redispatch).

In summary, the paper at hand contributes by combining the mentioned streams of studies. Thereby, typical limitations of existing studies in this field are overcome and more profound and realistic assessments are performed. The results do not comprise only an in-depth analysis of technical and socio-economic impacts of different PZCs (e.g. changes in dispatch schedules, redispatch amounts, shifts of generation between PZCs, changes in welfare and related redistributive effects); they also show how some of the shortcomings of FBMC can eventually be overcome by improved PZCs whilst the relevance of other FBMC features increases.

The remainder of this paper is organized as follows. Sec. 2 describes the developed methodology. This includes the process of identifying improved PZCs, but mainly explains the modeling of the stages of the market coupling (MC) process. Subsequently, Section 3 presents the case description, Section 4 continues with exhibiting the relevant results, and Section 5 draws the main conclusions.

5. More precisely, we model the combination of FBMC (as being applied in CWE) and NTC-based MC (as applied for the remaining European markets).

2. METHODOLOGY

2.1 Overall methodology

Figure 1 provides an overview of the used methodology which is summarized in the subsequent paragraphs (cf. also the contained references to subsections in Figure 1). The assessment starts with a (long-term) price zone reconfiguration process. Effectively, this encompasses the methodology of determining price zone delimitations. Therefore, we apply the hierarchical cluster algorithm developed in (Felling and Weber, 2018), which is shortly summarized in Section 2.2. This process yields a sequence of PZCs with different numbers of zones, out of which distinct PZCs are selected. For each PZC, a model chain is executed, that consists of a generation and structuring process of input data for the grid and market simulation (Section 2.3) and the simulation of the stages of the electricity market under the regime of FBMC, i.e. starting with the first stage two days before delivery (D-2) at which the FBMC parameters are determined (Section 2.4), followed by the day-ahead market (D-1) (Section 2.5) and the redispatch modelling in the real-time (D) stage (Section 2.6).

In Figure 16 in Appendix B, a more detailed flow chart of the full model chain is shown and shortly described. In general, the design approach has been to make use of proven models, extend these by new functions and features and develop a customized data handling environment. The use of several specialized models allows reproducing real-world system behavior and processes to a high level of detail.

After having simulated the three stages for each PZC, an important step is constituted by individual and combined assessments of the model outcomes. Therefore, the most relevant evaluating operations are described in Section 2.7.

Figure 1: Schematic illustration of the price zone reconfiguration process and its link to modeling and assessing short-term market processes.

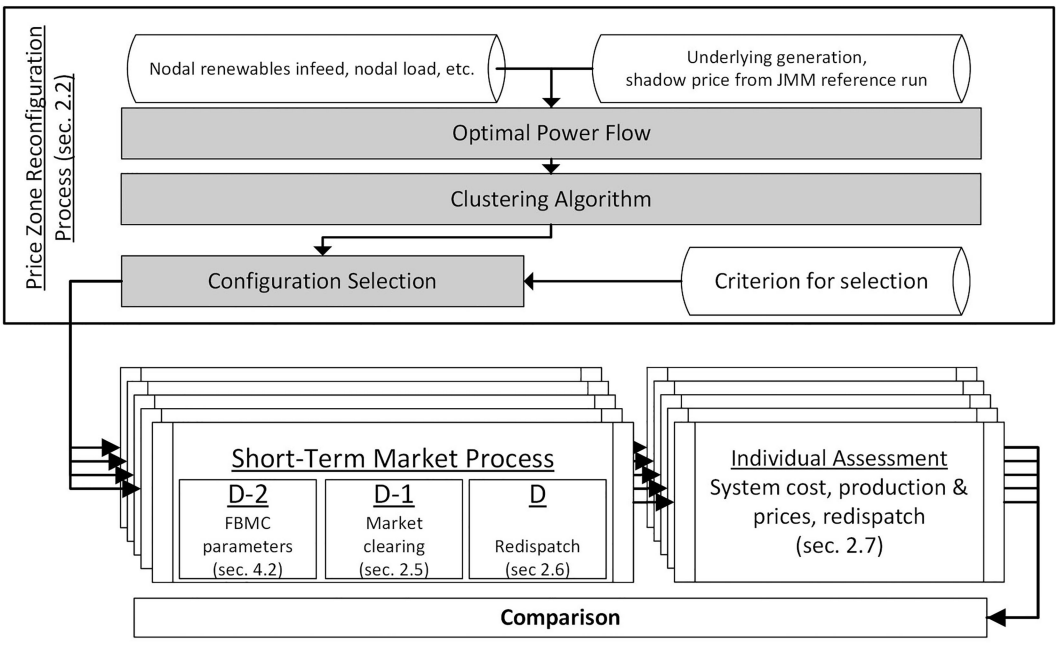

2.2 Price zone reconfiguration process

This section describes the method of identifying new PZCs as alternatives to the existing configuration. We apply the hierarchical cluster algorithm developed in Felling and Weber (2018) and therefore only summarize briefly the algorithm's main operations.

The algorithm clusters nodes to zones based on similarity of LMPs. Similarity of LMPs at two nodes implies that sufficient transmission capacity is available between these nodes. Hence, when determining possible price zones, nodes should be aggregated first where LMPs are most similar. Due to the hierarchical structure of the algorithm, it starts with the configuration in which every node corresponds to exactly one zone (nodal set-up) and ends when all nodes are grouped to one zone. In each stage of the clustering procedure, two zones are aggregated following a specific merging criterion being the least increase in price variation within zones V^{within}. This entails PZCs with individual zones having prices as homogeneous as possible and being delimited by lines that tend to be congested. In Felling and Weber (2018), the authors show that the total price variation in a system V can be decomposed into a variation between and within price zones ($V^{between}$ and V^{within}, respectively). Thus, in a nodal set-up (first iteration), the total price variation in the system, relative to V, is found between zones ($V^{between} / V = 100\%$) while in the last iteration, when all nodes form one zone, all price variations are within this zone ($V^{within} / V = 100\%$). The required LMPs are computed by the DC-lossless approximation of the optimal power flow (OPF) calculation based on Zimmermann et al. (2011) in a first step and then serve as input data for the clustering algorithm.

It is important to note that the algorithm proposed by Felling and Weber (2018) does not identify optimal price zone configurations in the sense that the selected configurations minimize the sum of market-based dispatch cost plus redispatch cost. Rather it is an approximate solution based on similar LMPs as indicators of absence of within-zone congestions. The solutions are moreover obtained through a greedy algorithm, which may converge to local optima (cf. the example in the Appendix of Felling and Weber, 2018). The formulation of an exact price zone optimization problem for a realistic large-scale system would already be demanding—as it would basically include all the elements of figure 16 in one optimization model. Solving such a model would be a daunting task—for a strongly simplified version, a heuristic solution has been proposed by Felling (2021).

2.3 Consistent input data generation

The first step of the core model chain is the generation and structuring of input data for the grid simulation as well as for the market simulation. It produces hourly time series of the so-called vertical load (i.e. electric demand minus renewables-based (RES) infeed and minus production of small-scale power plants) at each node. Especially power flow assessments require these input data at nodal level, while, for market simulations, the data are aggregated to zonal values.

Hourly regional demand values are calculated in a top-down approach; i.e. national demand time series are split into sector-wise time series (industry, service sector and households), taking yearly sector-wise demand and sector-wise hourly profiles into account. These time series are distributed to regions based on their share of sector-specific gross value added (GVA) or population respectively and their aggregation yields the regional demand time series. A detailed flow chart is given in Figure 17 in Appendix C.

Regional photovoltaic (PV) and wind infeeds are calculated in a bottom-up approach, using characteristic infeed profiles for each region based on measured data from local plants (PV) or simulated data (wind) using wind speeds (Deutscher Wetterdienst, 2017) at the position of known

local wind farms as well as their power curves and hub heights projected to the simulated year. This characteristic profile is scaled with the regional installed capacity. To make sure the model matches historical infeed on national level, a preliminary loop of the procedure is carried out for a historical year. In this first loop, the sum of the simulated regional time series of a country is compared to a national infeed time series of that year taken from literature. Thereby hourly scaling factors are calculated, which are then applied to the simulated time series in a second and final loop of the procedure for the actually considered year. A detailed flow chart is given in Figure 18 in Appendix C.

Generally, all individual time series are determined at the third level of Eurostat's NUTS classification (i.e. resulting in 642 regions × 3 time series × 8,760 h/a=16.9 million values) and then mapped to grid nodes. Offshore wind time series constitute an exception to this rule. They are calculated taking into account single wind parks. The Matlab-based program is a greenfield development made for combined grid and market modeling. It is optimized for handling large amounts of data and automatically sourcing the required data from the used meteo data base. A detailed description is given in Osinski et al. (2016).

2.4 Capacity allocation (D-2)

The second model step applied for each PZC is the capacity allocation. Two days before delivery (D-2), TSOs determine the parameters which define how much cross-zonal trade is allowable. These grid-based input parameters, namely PTDFs and remaining available margins (RAMs) are used in the clearing of the day-ahead market (D-1). For a detailed explanation of the full FBMC process, the user is referred to Amprion et al. (2014) and Felten et al. (2021). Here we focus on how the FBMC parameters are handled in our model framework, replicating the TSO procedures.

Such grid-focused processes are best handled in specialized tools like the open-source program MATPOWER (Zimmermann et al., 2011). This program has the advantage that certain functions are readily available and extensively tested (cf. Zimmermann and Murillo-Sánchez [2018] for comprehensive documentation). Using an open-source program has allowed us to develop customized functions. A typical data set of the capacity allocation model contains approx. 2,200 nodes, 3,500 lines and 700 transformers. This entails around 9 million nodal PTDF matrix elements. Using countries as price zones, the number of zonal PTDF elements is condensed to around 1,300.

Zonal PTDFs: Nodal PTDFs $A_{f,i}$ (of line f for net export at node i) can be calculated in MATPOWER based solely on the input parameters of the regarded grid (topology and susceptances). Zonal PTDFs $\overline{A}_{f,z}$ are determined by a weighted average of nodal PTDFs, with GSKs $\lambda_{z,i}^{inc,(p)}$ being the weights (distributing a change in net exports of a zone to nodes within that zone).

$$\overline{A}_{f,z} = \sum_{i \in I_z} \lambda_{z,i}^{inc,(p)} A_{f,i} \quad with \sum_{i \in I_z} \lambda_{z,i}^{inc,(p)} = 1 \tag{1}$$

According to Dierstein (2017), one of the most frequently applied GSK procedures is the GSK calculation proportional to installed dispatchable power plant capacities. In order to use one consistent GSK procedure for all FBMC regions, we use this procedure for all FBMC regions.

RAMs and base case: RAMs consist of four elements; the line capacity C_f, the line load offset $\Delta L_f^{(e)}$, the FRM M_f and the final adjustment value (FAV) V_f. They are distinguished by flow direction: standard flow direction (SFD/superscript *sfd*) and non-standard flow direction (NSFD/superscript *nsfd*).

$$R_f^{sfd} = C_f - \Delta L_f^{(e)} - M_f - V_f \tag{2}$$

$$R_f^{nsfd} = -C_f - \Delta L_f^{(e)} + M_f + V_f \tag{3}$$

$\Delta L_f^{(e)}$ incorporates the deviations of a nodal power flow model and a zonal power flow model with $q_i^{(e)}$ being the "expected" nodal net positions and $q_z^{(e)}$ the "expected" zonal net positions in the base case (cf. eq. 4). Thus, the expected line offset—if positive—reduces the available free line capacity.[6]

$$\Delta L_f^{(e)} = \sum_{z \in Z} \sum_{i \in I_z} A_{f,i} \left(q_i^{(e)} - \lambda_{z,i}^{inc,(p)} \overline{q}_z^{(e)} \right) \tag{4}$$

However, the market outcome depends on the FBMC parameters. Autoriteit Consument & Markt et al. (2015) call this a circular problem. TSOs have found a workaround by using a reference day. This seems expedient if especially two conditions are fulfilled. First, the number of FBMC price zones needs to be limited. Currently, this is the case with CWE containing five price zones. This aspect results in a small set of "likely corners" of the zonal FR, which reduces complexity of choosing such a reference day. Second, sufficient and consistent historical data needs to be available. For model-based assessments, however, both conditions are hardly fulfilled. In particular, such models are often used to analyze alternative market designs, policy choices and future scenarios. This includes possibilities like a drastically higher number of price zones or structural changes in fundamental factors (e.g. renewables expansion, conventional capacity decrease, etc.). Thus, we use a slightly different procedure to establish the best D-2 estimate. For doing so, we use the optimal power flow (OPF) function of MATPOWER (Zimmermann and Murillo-Sánchez, 2018). In the nodal EMCP, line capacities of intra-zonal lines can be increased to a level where the corresponding LFCs never become binding. If doing so, only inter-zonal lines are relevant and zones are free of congestion. Hence, this modified EMCP describes a zonal clearing. Thereby, we use the same data set as for detailed grid assessments with the exception of the capacity modification for intra-zonal lines. The result is a reasonable estimate of a zonal market outcome. The neglection of intra-zonal LFCs is in line with the current TSO procedures for estimating the base case. The TSOs' use of the market outcomes of a reference day also implies that intra-zonal constraints and redispatch are not considered forthe base case.

With regard to the base case estimation, the selection of considered intra-zonal load flow constraints (LFCs) and the FRMs used for the calculation of RAMs, we perform sensitivity calculations. Subsequently, we first discuss the settings of the assessed reference case. Thereafter, we explain the investigated sensitivities. In general, the sensitivities are defined by changing exactly one feature of the reference case. All other features remain unchanged.

Reference case For the reference runs, we use a base case that is characterized by perfect foresight of the theoretically possible renewable generation,[7] i.e. there is no deviation between the renewables forecast two days ahead of delivery (D-2) and its actual realization at the day of delivery (D). In terms of considered LFCs, the reference case does not consider any intra-zonal lines. Furthermore, in the reference case and all sensitivities, FRMs are based on a percentage value of the line capacity. For the reference case, this percentage value is set to 12%.

Base case sensitivity (ImpFS) We investigate the influence of forecast errors of renewables generation by considering imperfect information at the D-2 stage. The relative forecast errors are cal-

6. For more detailed explanation, we refer to Felten et al. (2021).

7. The term "theoretically possible" refers to the renewables infeed that is possible at plant level. That is to say the value does not consider any restrictions that may be imposed by the grid.

ibrated using historical forecast errors of the respective TSOs for the year 2017 (Entso-E, 2018b). These relative forecast errors are then applied to the used infeed time series yielding absolute forecast deviations. For the market clearing, the actual realizations are used.

Intra-zonal line sensitivity 1 (5%-PZC) Commonly, TSOs have considered intra-zonal lines to be significant when they feature any zone-to-zone PTDF with an absolute value greater than 0.05 (Amprion et al., 2014). In this sensitivity, we apply this criterion for each PZC. Thus, we calculate the zonal PTDFs and all zone-to-zone PTDFs for each PZC. If the threshold of 0.05 is exceeded at least once for an intra-zonal line, the corresponding LFCs are considered. Henceforth, we refer to this sensitivity as 5%-PZC.[8]

Intra-zonal line sensitivity 2 (5%-BAU) For calculating whether an intra-zonal line exceeds said 5% threshold or not, the only input parameters are (nodal) PTDFs and GSKs. Notably, other factors like the levels of net exports of zones and line capacities are no input parameters to the calculation. However, latter factors were implicitly considered in the process of establishing the 5% threshold, as the TSOs determined it by testing various alternative threshold values (Amprion et al., 2014). This was done under consideration of the given PZC, i.e. under use of corresponding net export levels and line capacities. When considering alternative PZCs, the standard deviation of zonal PTDFs increases. As the worst-case zone-to-zone PTDF is subject to assessment, using the 5% threshold tends to result in a high number of intra-zonal constraints even though critical zone-to-zone trades tend to be smaller and, thus, the line capacities can be expected to be sufficient in many situations. In order to avoid this bias, we define the sensitivity 5%-BAU. In this sensitivity, the LFCs of the set union of the lines considered for the business-as-usual configuration (BAU-C) and the inter-zonal lines of the regarded PZC are considered. Thus, the set of intra-zonal lines is not empty (as in the reference case) but, at the same time, not as large as in 5%-PZC.

FRM sensitivity As mentioned in Section 1 and introduced in Felten et al. (2021), FRMs are used to account for uncertainties between the D-2 and D-1-stage and approximations induced by GSKs and the base case assumption. However, when reducing the number of zones, uncertainty in zones decreases, which should justify the use of lower FRM values. That is why, in this sensitivity, we do not keep the FRM values constant anymore. Instead, we decrease the percentage value for FRM calculation reciprocally to the number of zones. In order to attain 12% for the BAU-C, the FRM equals 60% divided by the number of zones. That yields 12% for the BAU-C and, for instance, 1.2% for a PZC with 50 zones.

2.5 Day-ahead and intraday market clearing

The third model step replicates the market processes. Prior to simulating the actual bidding on electricity markets, the constraints from combined heat and power (CHP) provision are determined separately. This is important as many European countries are characterized by high shares of CHP and as heat scheduling typically takes place ahead of electricity market clearing (cf. Nielsen et al., 2016; Varmelast, 2018). For this purpose, we use a separate CHP model. In a first step, this tool models the heat demand of district heating grids. In a second step, it determines the heat extraction from CHP plants, which then can be translated into minimum and maximum electricity generation

8. Note that, according to the aforementioned "Clean Energy Package", internal lines should not be considered as LFCs in the market clearing in the future. However, they can still be considered as contingencies, i.e. potential outages, to approximate n-1 security (Amprion et al., 2019).

bounds for these units. The model is documented in Felten (2020) and has proven suitable for power system planning (50Hertz et al., 2018).

For modeling the market clearing, the WILMAR Joint Market Model (JMM) is used. A comprehensive description of this scheduling model is given in Meibom et al. (2006) and some of its applications are presented in Tuohy et al. (2009); Meibom, P. et al. (2011); Trepper et al. (2015). The model is based on the assumption of a competitive market and (as used here) inelastic demand. Thus, the market outcome corresponds to the result of a central cost minimization. The JMM has more than 40 constraint types, a typical JMM run takes into account around 17,000 power plants, grouped into around 700 plant classes. From 2.4, we already know that a typical PTDF matrix of the JMM alone has 1,300 elements. These constraints implemented in the JMM are much more complex than those used for theoretical analyses as in Bjørndal and Jörnsten (2001); Bjørndal et al. (2003); Ehrenmann and Smeers (2005); Bjørndal and Jörnsten (2007); Androcec and Krajcar (2012); Neuhoff et al. (2013); Oggioni and Smeers (2013); Grimm et al. (2016a); Grimm et al. (2016b) or in Felten et al. (2021).[9]

A model development that constitutes a major contribution of this paper is the consideration of FBMC in a large-scale market model. This statement especially refers to three aspects. First, we make use of input data from large-scale yet specialized and very detailed models. Another choice could have been to implement a simplified (e.g. aggregated) grid model in the JMM. This alternative choice could have reduced model interfaces whilst entailing losses in accuracy. Therefore, we have focused on interface design with the goal of most realistic FBMC constraint parametrization. Second, large-scale modeling does not only refer to CWE. Price zones in CWE are not isolated from the other European markets. The regional scope used in the JMM comprises entire continental Europe plus Scandinavia, UK and Ireland and excludes member states of the former Soviet Union. Thus, the effect of interlinked European markets is reproduced. Third, until now, FBMC is only carried out between price zones in CWE. MC with and between markets outside of CWE is still performed by means of NTC-based MC. The JMM developments have taken this into account. As part of the case definition of the JMM, zones can be assigned to the subset Z_{FB}. The commercial exchanges between pairs of these zones ($(z,z') \in Z_{FB} \times Z_{FB}$) are then subject to FBMC. Cross-zonal exchanges between the remaining zone pairs ($(z,z') \in \{\{Z \times Z\} \setminus \{Z_{FB} \times Z_{FB}\}\}$) are managed on basis of NTCs. This user-defined allocation of zones to the set Z_{FB} does not only allow us to model the current set-up, it also enables us to simulate future scenarios where further price zones use FBMC. The resulting LFCs are given in eq. 5 to 7. This formulation differs from the theory of zonal FBMC in Felten et al. (2021) as it uses bilateral exchanges $e_{z,z',t}$ instead of net exports $\overline{q}_z$. This simply allows us to use the established variables of bilateral exchanges for both MC methods.

$$e_{z,z',t} = e^{DA}_{z,z',t} + \Delta\, e^{ID,+}_{z,z',t} - \Delta\, e^{ID,-}_{z,z',t} + e^{nonsp,+}_{z,z',t}$$
$$\forall\, t \in T^{¨}\ ,\ \forall\, (z,z') \in Z \times Z \tag{5}$$

$$R^{nsfd}_{f,t} \le \sum_{z} \overline{A}_{f,z,t} \left(\sum_{z'} e_{z,z',t} - \sum_{z'} e_{z',z,t} \right) \le R^{sfd}_{f,t}$$
$$\forall\, f \in F_{cb}, \forall\, t \in T, \forall (z,z') \in Z_{FB} \times Z_{FB} \tag{6}$$

9. With regard to JMM developments, the must-run constraints of CHP plants have been implemented in the course of the present work. This is said for the sake of completeness, as the constraints differ from Meibom et al. (2006), but this is not in the focus of this paper.

$$0 \leq e_{z,z',t} \leq e^{max}_{z,z',t}$$
$$\forall t \in T^{opt}, \forall (z,z') \in \left\{\{Z \times Z\} \setminus \{Z_{FB} \times Z_{FB}\}\right\} \quad (7)$$

$$e^{DA}_{z,z',t}, \Delta e^{ID,+}_{z,z',t}, \Delta e^{ID,-}_{z,z',t}, e^{nonsp,+}_{z,z',t} \geq 0$$
$$\forall t \in T^{opt}, \forall (z,z') \in Z \times Z \quad (8)$$

Eq. 5 thereby gives the components of the bilateral exchange variable $e_{z,z',t}$, eq. 6 provides the LFCs for FB-coupled price zones, eq. 7 constitutes the NTC (and non-negativity) constraint for $e_{z,z,t}$, and eq. 8 summarizes the nonnegativity constraints of the components of $e_{z,z',t}$.

Since the JMM depicts almost the complete European electricity market, the linear deterministic program version is chosen in this case study in order to keep calculation times manageable. This especially entails that generators are grouped to so-called unit groups (i.e. groups of units of same technological type, using the same fuel, having similar ages and being located in the same PZ). Using the deterministic set-up implies that power plant operators are modeled to have perfect knowledge of renewables-based generation and power plant availabilities at the day-ahead bidding stage (D-1 stage). Such perfect knowledge basically represents an upper bound for the bidding performance of the power plant operator and, having inelastic demand, for the welfare achievable through the market clearing process under the given constraints. It further entails that day-ahead and intraday clearing results are almost identical. Hence, we refer to the results of both (day-ahead and intraday) as scheduled dispatch or market outcomes, even though, formally, intraday market clearing would correspond to the D stage of the market. It is important to note that the deterministic setting of the JMM only concerns the bidding and market clearing process under use of given constraints. The exchange capacities that are allocated to the market at the D-2 stage are not derived using perfect foresight. As explained in Felten et al. (2021), the FBMC procedures can yield inaccurate LFCs in various ways and, therefore, constraints used in the market clearing are not perfect. This also constitutes one focus area of our case study in Section 3 to 5. It should also be noted that the model assumes that market participants bid truthfully, not trying to profit from potentially predictable price differences between the D-1 and D stage. In CWE, redispatch is highly regulated and essentially cost-based and, therefore, incentives for strategic bidding are small.

2.6 D stage: Redispatch

In order to model the processes at the D stage, we have developed a novel redispatch model. The basic principle of redispatch can be described as follows. Once the markets have been cleared, dispatch schedules (and updated renewables forecasts) are known to the TSOs. From these schedules, corresponding line loadings can be calculated. If line overloads result from the scheduled dispatch, TSOs must take measures to ensure the safe and reliable grid operation. In this case, the by far most frequent measure is the interference of the TSO in the dispatch schedule of power plants, i.e. redispatch (including renewables curtailment) (BNetzA and Bundeskartellamt, 2018). Thus, the responsible TSO identifies adjustments to power plant dispatch that reduce critical line loadings and, in sum, avoid overloads. Interference into the dispatch schedule also impacts the economics of power plant operators. Therefore, generators are reimbursed or need to pass on avoided operational costs. This is explained as follows:

1. **Positive redispatch** $\Delta g^{+}_{u,t} > 0$: Increasing the generation of power plants downstream of an overloaded line reduces its critical loading. For ramping up and operating these plants, additional costs are incurred by power plant operators, and these need to be reimbursed by the responsible TSO. Apart from the variable costs of steady-state operation $c_{u,t}$, cost of start-up fuel, start-up degradation costs, etc. exist. As only additional costs are reimbursed to instructed power plant operators, the contribution margins of this operation is 0. Thus, overall producer rents remain unchanged from those attained on the markets. From a system perspective, reimbursed costs add to the market clearing costs (i.e. the costs accrued as per day-ahead schedule).
2. **Negative redispatch** $\Delta g^{-}_{u,t} > 0$: Generation of power plants upstream of an overloaded line aggravates its critical loading. When these generators are ordered to reduce generation, they remain with the revenues from previous power sales. However, they need to pay the saved variable costs $c_{u,t}$ minus additional cycling and other costs to the TSO. In essence, generators should remain with their contribution margins which they would have attained through the scheduled dispatch. Thus, also in case of negative redispatch, producer rents are not changed. From a system perspective, only the amount payable from the power plant operator to the TSO reduces redispatch costs. In case of renewables curtailment, the economics are different in one major aspect. The curtailment causes a reduction of revenues which mostly stems from lost payments according to renewables support schemes and, therefore, renewables curtailment is usually more costly than redispatch of non-renewables-based power plants.

The German legislation on this topic (Oberlandesgericht Düsseldorf [OLG], 2015) reveals that redispatch reimbursement and chargeable costs have numerous elements (e.g. opportunity revenues from sales at different markets, lost entitlement to regulatory payments, cost of alternative heat supply, etc.) and that special arrangements are allowed. The exact reimbursement/cost figures are not public. Therefore, in the redispatch model, we use a term γ_u to model the costs that come in addition to $c_{u,t}$. We set γ_u to 0.2, i.e. reimbursable costs for positive redispatch are 20% higher than $c_{u,t}$ and chargeable costs for negative redispatch are 20% lower than $c_{u,t}$. A rough estimate like this helps to overcome non-existence of publically available actual cost data. However, a factor like γ_u has influence on model results. In order to assess the sensitivity of our model to γ_u, we perform a sensitivity analysis in Appendix E.

In line with the previous statements, the optimization problem is stated in eq. 9 to 21. Precedent to this, we define the used sets and variables and explain the input parameters and the reasoning behind the objective function and restrictions.

2.6.1 Redispatch objective

The objective of the responsible TSOs (and of the developed redispatch model) is to avoid line overloads while causing least additional system costs possible. Thus, the scheduled dispatch $g_{u,t}$ for all hours of the year T is handed over from the JMM to the grid model. A power flow calculation is performed in MATPOWER (Zimmermann et al., 2011) in order to detect line overloads. Subsequently, redispatch amounts are determined using the cost-minimizing objective in eq. 9 for all hours with (scheduled) overload situations T^{RD}. Therein, $\Delta g^{+/-}_{u,t}$ denote positive/negative redispatch amounts, $c^{+/-}_{u,t}$ the corresponding specific reimbursable/chargeable costs (described under numerals 1 and 2 above). We explain the optimization problem in detail in Section 2.6.3 below. For now, it is sufficient to note that the formulated redispatch problem can be understood as cost-based redispatch.

2.6.2 Sets of power plant units and parameters of the redispatch model

It is important to distinguish between different power plants. The distinctions are made in terms of technical availability, applicability of regulatory regimes, operational states (according to the scheduled dispatch) and in terms of combinations of aforementioned aspects. As they generally depend on the operational state as per dispatch schedule, some unit sets are time dependent (index *t*). The set of all units is denoted by $\mathcal{U}$. For brevity, the reader is referred to Appendix A for a complete list of unit subsets mentioned above and used in eq. 13 to 26.

We utilize the market outcome determined in the JMM as input parameters for the redispatch model. This comprises not only the scheduled dispatch but also the outcome of the different reserve markets and the shadow prices of hydro power plants. Furthermore, the scheduled heat extractions $h_{u,t}^{chp}$ of CHP plants are considered, as they restrict the redispatch ability further. $h_{u,t}^{chp}$ is the output of the CHP tool described in Felten (2020). One parameter that should be briefly explained is $g_{u,t}^{started}$. In the JMM, it has several purposes (cf. Meibom et al., 2006). The most important one is to model intertemporal constraints of unit groups, such as shutdown or operating periods, that have to last for a minimum number of consecutive hours. Thus, for the redispatch model, only part of the unit group is in operation (started) and, in case of slow units, only this started capacity is available for positive redispatch. At the same time, the technical minimum load is also determined by means of $g_{u,t}^{started}$ (cf. eq. 18).

2.6.3 Redispatch optimization problem

With the above definitions, the optimization problem in eq. 9 to 21 can be formulated as follows:

$$min_{\Delta g_{u,t}^{+},\Delta g_{u,t}^{-}} \sum_{t\in T^{RD}} \sum_{u\in\mathcal{U}} (c_{u,t}^{+}\Delta g_{u,t}^{+} - (c_{u,t}^{-} - c_{t}^{max})\Delta g_{u,t}^{-}) \tag{9}$$

s.t.

$$\sum_{i\in I} A_{f,i} q_{i,t}^{RD} \leq C_f \forall\ f \in F, t \in T^{RD} \tag{10}$$

$$-\sum_{i\in I} A_{f,i} q_{i,t}^{RD} \leq C_f \forall\ f \in F, t \in T^{RD} \tag{11}$$

$$q_{i,t}^{RD} = \sum_{u\in U} b_{u,i}(g_{u,t} + \Delta g_{u,t}^{+} - \Delta g_{u,t}^{-}) - d_{i,t} - \Delta g_{i,t}^{mbc} \forall\ i \in I, t \in T^{RD} \tag{12}$$

$$\Delta g_{u,t}^{+} \leq g_{u,t}^{started} - g_{u,t}^{spin,+} - g_{u,t}^{nonsp,+} - \delta_u h_{u,t}^{chp} - g_{u,t} \forall\ t \in T^{RD}, u \in \mathcal{U}^{RD,slow} \tag{13}$$

$$\Delta g_{u,t}^{+} \leq g_{u,t}^{max} - g_{u,t}^{spin,+} - g_{u,t}^{nonsp,+} - \delta_u h_{u,t}^{chp} - g_{u,t} \forall\ t \in T^{RD}, u \in \mathcal{U}^{RD,fast} \tag{14}$$

$$\Delta g_{u,t}^{+} \leq g_{u,t} - g_{u,t}^{spin,+} - g_{u,t}^{nonsp,+} \forall\ t \in T^{RD},\ u \in \mathcal{U}^{ps,pump} \tag{15}$$

$$\Delta g_{u,t}^{+} = 0 \ \forall\ t \in T^{RD}, u \in \mathcal{U}^{noRD,pos} \tag{16}$$

$$\Delta g_{u,t}^{-} \leq g_{u,t} - \sigma_u h_{u,t}^{chp} - g^{spin,-} \forall\ t \in T^{RD}, u \in \mathcal{U}^{RD,neg} \tag{17}$$

$$\Delta g^{-}_{u,t} \leq g_{u,t} - \kappa_u g^{started}_{u,t} - \delta_u h^{chp}_{u,t} - g^{spin,-} \forall\ t \in T^{RD}, u \in \mathcal{U}^{RD,neg} \tag{18}$$

$$\Delta g^{-}_{u,t} \leq g^{max}_{u,t} - g^{spin,-}_{u,t} - g^{nonsp,-}_{u,t} \forall\ t \in T^{RD},\ u \in \mathcal{U}^{ps,pump} \tag{19}$$

$$\Delta g^{-}_{u,t} = 0\ \forall\ t \in T^{RD}, u \in \mathcal{U}^{noRD,neg} \tag{20}$$

$$\sum_{u \in U} \Delta g^{+}_{u,t} = \sum_{u \in U} \Delta g^{-}_{u,t} \forall\ t \in T^{RD} \tag{21}$$

The optimization problem is solved in MATPOWER under use of the DC-OPF function (cf. (Zimmermann et al., 2011).[10] Apart from the non-negative decision variables for the positive and negative redispatch amounts $\Delta g^{+/-}_{u,t}$, only the nodal net export after redispatch q^{RD}_i constitutes a (dependent) variable. Notably, line ratings are reduced to 85% of their capacity to approximate n-1 security. All other symbols in eq. 9 to 26 denote parameters to the redispatch problem. Eq. 10 and 11 describe the physical LFCs, which limit the line loadings of all lines $f \in F$. Eq. 12 describes the nodal net exports after redispatch. Eq. 13 to 16 constitute the constraints for positive redispatch applicable to distinctive sets of units. Eq. 17 to 20 are the analogous constraints for negative redispatch. Eq. 21 ensures the energy balance (cf. Felten et al., 2021). In addition to the aforementioned cost terms, the objective function contains a further term c^{max}_t. Otherwise, a straightforward cost-minimizing problem would perform a re-optimization of the scheduled dispatch. That is, in some situations, the grid model would identify nodal dispatch improvements in order to reduce costs (in addition to relieving anticipated overloads). The reason is that the JMM models technical restrictions on power plant level in much more detail. For instance, intertemporal constraints can cause power plants to operate even though these power plants may temporarily not be in the money. These constraints are real-world restrictions which are represented in the JMM in more detail than in the redispatch model (cf. Meibom et al., 2006). Considering these technical powerplant constraints in the grid model in addition to the detailed grid constraints would increase the computational complexity significantly. The model would become a MIP instead of a LP problem. Another example for possible re-optimization is given by LFCs in the market clearing. Felten et al. (2021) demonstrate that the market clearing problem in an FBMC zonal market design can be subject to unnecessarily restrictive LFCs and only has limited means to manage intra-zonal congestion. This can lead to suboptimal market outcomes. As the grid model considers the exact LFCs and can manage intra-zonal congestion on nodal level, an OPF tends to improve grid utilization and congestion management. As redispatch is not executed for cost-minimizing purposes, we adjust the redispatch problem so that any such re-optimization of market outcomes in an OPF is avoided. This is done by including c^{max}_t in the objective function (eq. 9). c^{max}_t denotes the variable costs of the most expensive generator. Thus, for purposes of the optimization, negative redispatch is modeled to cause additional costs at a marginal value of $c^{max}_t - c^{-}_{u,t}$, and these costs have the reverse order of the variable costs of the generators. Thereby, the variable costs of power plants are derived as shown in eq. 22 to 25. For thermal power plants, eq. 22 expresses the marginal costs of generation as a linearization of the total cost increase $\Delta C_{u,t}$ relative to the generation increase $\Delta g_{u,t}$. This yields different costs for plants starting from zero-generation and from part load. Hence, the effect of low part load efficiencies is

10. For the mathematical description, we neglect variables that can be used for grid topology changes, as we do not consider such changes in this paper (except for phase shifting transformers). Furthermore, we use the PTDF notation because it is analogue to Section 2.4 and 2.5 and, under the used simplifications, mathematically equivalent to the formulation with voltage angles.

considered through eq. 22. With regard to variable costs of pumped storage (eq. 24 and 25), we use the opportunity cost rationale described in Steffen and Weber (2016).

$$c_{u,t} = \frac{\Delta C_{u,t}}{\Delta g_{u,t}} \qquad \forall\, u \in \{\mathcal{U}^{disp} \setminus \mathcal{U}^{hydro}\} \tag{22}$$

$$c_{u,t} = \mu^{hyr}_{u,t} \qquad \forall\, u \in \mathcal{U}^{hyr} \tag{23}$$

$$c_{u,t} = \mu^{ps}_{u,t} + \mu^{ps}_{u,t} \frac{1-\eta^{ps}_{u}}{1+\eta^{ps}_{u}} \qquad \forall\, u \in \mathcal{U}^{ps\ turb} \tag{24}$$

$$c_{u,t} = \mu^{ps}_{u,t} - \mu^{ps}_{u,t} \frac{1-\eta^{ps}_{u}}{1+\eta^{ps}_{u}} \qquad \forall\, u \in \mathcal{U}^{ps,pump} \tag{25}$$

$$c_{u,t} = c^{curt} \qquad \forall\, u \in \mathcal{U}^{res} \tag{26}$$

2.7 Main assessments of model outcomes

The relevant results can be broken down into market outcomes and redispatch results. The corresponding evaluation steps are explained as follows.

Market results: The JMM delivers results on all relevant market outcomes, i.e. electric and thermal generation by fuel and by unit group, electricity prices, exchanges, generation costs, producer and consumer rents, etc. In this study, we focus on three main issues.

Firstly, we are interested in the welfare changes. I.e. we investigate changes of the total operational costs as per scheduled dispatch. Hereinafter, we refer to these costs as market clearing costs (MCC). These costs comprise all variable costs of generators (e.g. fuel and CO_2 costs and variable operation and maintenance costs). We adjust this term by the value of final water reservoir filling volumes. As final filling levels of reservoirs may vary for different PZCs, this decreases/increases the opportunity to achieve future revenues. The valuation is made at the final opportunity costs of water in the corresponding price zone (PZ) of the reference configuration.[11] Decreases in MCC after the water value adjustment[12] correspond to welfare increases as per market clearing. These results are reported in Section 4.1. Note that our methodology enables us to compute the short term changes in welfare for a given generation capacity mix. We do not assess the longer term impacts of different PZCs, including notably their impacts on investments (cf. e.g. Ambrosius et al., 2020; Grimm et al., 2021). Second, as welfare changes are not equally distributed to involved parties, (i.e. consumers, producers and network owners), these redistributive effects constitute a major issue of alternative PZCs. Therefore, the changes in consumer, producer and congestion rents at country level are analyzed.[13] Thus, we map the rents of PZs back to countries, by weighting con-

11. As the opportunity for electricity sales from hydro generation in the Nordic countries is significantly reduced in all improved PZCs (cf. Section 4.2.1), we use the final water value of a PZC with a medium number of PZs (8-ImpC) for the adjustment.

12. For brevity, we do not explicitly state the water value adjustment henceforth. However, it always is included.

13. Note that changes in consumer rents are well-defined even for price inelastic demand and are computed here as in Spiecker et al. (2013) or Trepper et al. (2015). Spiecker et al. (2013) provide a graphical illustration on the computation of changes in rents, whereas details on the calculation of consumer rents and other rents are discussed in Ovaere et al. (2016).

sumer rent and congestion rent by demand and by adding up contribution margins of plants. Another result of interest is the scheduled dispatch. Each unit group's schedule is taken and disaggregated to units, which serves as input for the redispatch model (cf. Section 2.6) and for further analyses (cf. Section 4.2.1).

Redispatch results: The assessment of technical outcomes of the redispatch model is straightforward. Values for $\Delta g_{u,t}^{+/-}$ result from the optimization problem presented in Section 2.6.3 and can be broken down by fuel, node, time, etc. Furthermore, scheduled line overloads and free capacities on lines are a result of the initial power flow calculations of the redispatch model. In terms of assessment of redispatch costs (RDC), there is one relevant aspect. In the objective function of the redispatch model (eq. 9), we have used c_t^{max} to avoid re-optimization of market outcomes. However, the term $\sum_{t \in T^{RD}} \sum_{u \in \mathcal{U}} c_t^{max} g_{u,t}^{-}$ serves for OPF purposes only. Thus, we use the objective value of the redispatch problem reduced by $\sum_{t \in T^{RD}} \sum_{u \in \mathcal{U}} c_t^{max} g_{u,t}^{-}$ for the purpose of RDC assessment. Notably, the factor γ_u is an important parameter when determining RDC. Thus, we provide a sensitivity analysis for different γ_u values in Appendix E.

3. CASE STUDY DATA

In this section, we describe the most relevant data assumptions for our case study. Table 1 gives an overview of the relevant power plant data assumptions. The case study is performed for the year 2020. In the following, the corresponding sources are explained further. The power plant data are based on the Platts power plant database (S & P Global Platts, 2018). The data have been updated continuously and enhanced by further input data (e.g. agency data such as BNetzA, 2018; or TSO data such as 50Hertz et al., 2014) and plant-specific research mainly relying on plant owners' web presence and press releases. Commissioning and decommissioning dates of 2018 to 2020 are assumed as per actual announcements and official plannings (e.g. 50Hertz et al., 2014). Aggregate installed capacities for conventional power plants and renewables-based generators (cf. Table 1) are adjusted to match the trend scenario of Entso-E's System Outlook and Adequacy Forecast (Entso-E, 2015).

Table 1: Overview of capacities and renewables assumptions for the year 2020.

	AT	BE	CH	DE	FR	LU	NL
Installed Capacity [GW]							
Biomass	0.12	1.71	0	6.39	0.97	0	0.49
Hard coal	0.35	0.02	0	27.63	2.81	0	4.75
Hydro	10.58	0.1	12.11	3.95	21.11	0.04	0.04
Lignite	0	0	0	17.05	0	0	0
Natural gas	5.12	5.65	0.25	25.88	12.4	0.44	19.57
Nuclear	0	5.06	2.80	8.11	63.00	0	0.49
Other	0.16	0.11	0.31	6.35	3.18	0	0.18
Pump storage	4.73	1.44	3.13	7.78	4.09	0	0
Yearly Production [TWh]							
Solar	2.4	3.6	1.7	42.9	10.9	0.1	5.6
Wind offshore	0	7.4	0	26.8	4.2	0	3.9
Wind onshore	9.1	6.0	0.2	93.1	28.6	0.2	10.0

The time series data are generally based on the year 2012, while absolute annual values are projected to the year 2020. National renewables and demand profiles for 2012 are based on TSO data (Open Power System Data, 2019; Elia, 2016). The yearly electric demand per sector and coun-

try as shown in Table 7 in Appendix D is taken from IEA Electricity Information (IEA, 2014) and assumed to stay constant over the years. The generation of regional renewable and load time series as explained in Section 2.3 is based on a broad range of publications from national ministries, offices and TSOs. Table 6 in Appendix D gives an overview of the used sources.

We use quotations for fuel and CO_2 futures at the European Electricity Exchange (Energate, 2018); i.e. three-month-average notations of traded 2020 (or latest available[14]) futures product for coal, natural gas, fuel oil and light oil as well as for CO_2 prices. The price for lignite is based on values used in the German Grid Development Plan (50Hertz et al., 2014). Fuel costs and CO_2 prices are shown in Table 8 and variable costs of power plants in Table 9 in Appendix D.

While our market simulations comprise almost entire Europe, in order to cope with interdependences across Europe, the transmission grid is modeled for the extended CWE area (CWE+, i.e. Austria, Belgium, France, Germany, Luxembourg, the Netherlands and Switzerland) including the 220- and 380-kV voltage levels. In parts of Germany, 110-kV transformers are also modeled. The grid model is based on a set of publicly available data ("static grid model") (APG, 2017; RTE, 2015; TenneT TSO GmbH, 2015), but we made individual improvements and adjustments to these models according to additional information obtained from TSOs. Moreover, we added lines according to the national grid development plan in Germany (50Hertz et al., 2014) and of the EU (Entso-E), 2014). For the analysis, we use the electricity grid of the year 2016 as a base line (start of the case set-up). This is equivalent to assuming delays in grid extension of up to 4 years. In total, over 2,200 nodes, 3,600 branches and 600 transformers are modeled.

4. RESULTS

This section presents and discusses key findings of our approach. First, we present the results of the cluster algorithm, i.e. the improved PZCs in Section 4.1. Subsequently, we investigate the reference case and exemplarily highlight the impact of a specific reconfiguration on market and redispatch results. The same section includes a discussion on the distribution of welfare changes (cf. Section 4.2.3). Thereafter, the investigated sensitivities conclude Section 4.

4.1 Price zone reconfiguration

The hierarchical clustering algorithm yields 2226 PZCs, what corresponds to one PZC for each merger of zones ($card(I)$—1 = 2226). As explained in Section 2.2, the objective function of the algorithm is to minimize the within-zone variation V^{within}. Thus, we use V^{within} / V as selection criterion for PZCs for a given number of PZs. Figure 2 shows how the normalized within-zone variation V^{within} / V decreases with the number of PZs. Moreover, the threshold values which are used to select PZCs for further investigations are indicated in Figure 2.

The thresholds of 15%, 10%, 5% and 2.5% correspond to PZCs with 8, 14, 28 and 50 zones, respectively. In addition, we assess the existing PZC with 5 PZs, which we call business-as-usual configuration (BAU-C) henceforth. As explained in Section 2.2, we also consider an improved 5-zone configuration obtained from the clustering algorithm for our assessment. The improved

14. The notations were taken at the time when setting up the case study data, i.e. April to June 2015. In case trade of a 2020 futures product had not started at this time, we used the latest available futures product.

Figure 2: Normalized values for V^{within} as a function of the number of zones.

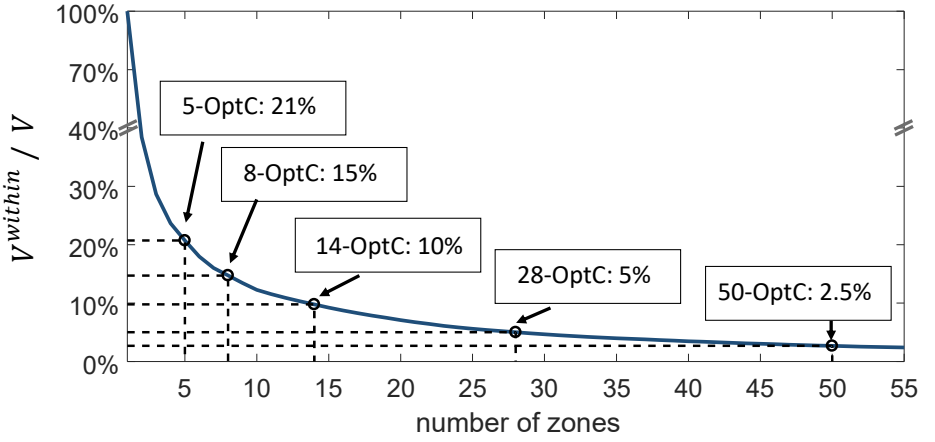

PZCs are denoted 5-ImpC, 8-ImpC and so forth. Figures 3 to 8 illustrate the geographical scopes of the PZs for all assessed PZCs.[15]

One immediate observation is that—except for large parts of French borders—national borders do not align with improved PZ delimitations. Notably, the German-Austrian PZ splits apart and new PZs in Eastern Austria and Northern Germany emerge already in the 5-ImpC.

4.2 Results of the reference case

The impacts of these altered PZCs on overall system costs, i.e. market results and redispatch,[16] are presented in Figure 9. Therein, the change in annual MCC and RDC are shown. The quantities are always compared to the BAU-C. The sum of both values is labelled system cost (SC) increase/decrease and is also given in Figure 9. SC decreases correspond to short-term welfare increases which result from improved PZCs. However, when analyzing the results, one has to keep in mind that the identified PZCs are obtained via a heuristic and, thus, might not be optimal. There might be better suited PZCs for the different numbers of zones (cf. Felling and Weber, 2018). Algorithms based on nodal prices to identify price zones are criticized in Ambrosius et al. (2020) and Felling (2021). Moreover, the objective function of the clustering algorithm aims at minimizing price variations and not explicitly overall system costs. An algorithm based on the overall system costs and a comparison to the algorithm based on nodal prices is given in Felling (2021). However, the applied algorithm based on nodal prices is similar to the technique used in the official first Bidding Zone Review (Entso-E, 2018a). Thus, not only the presented results here but any assessment of PZCs based on nodal prices should be interpreted with care.

All improved configurations achieve lower SC than the BAU-C. The savings are mainly achieved by monotonically decreasing RDC. On the other hand, MCC are always higher than in the BAU-C. Yet, no clear trend is observable for MCC when increasing the number of PZs. Both effects (MCC and RDC changes) add up to a non-monotonic decrease in SC with an increasing number of

15. Notably, the cluster algorithm ensures, that all nodes within a zone are connected. In case zones appear to be unconnected (e.g. Zone 28 in figure 8), these are artifacts of the representation using a Voronoi diagram. This happens for example, if a long 380 kV line connects two nodes that are in one zone, but close to this interconnecting line there are still 220 kV nodes or stubs that belong to another zone.

16. A brief overview over computation times is given in Appendix 12.

Figure 3: BAU-C.[17]

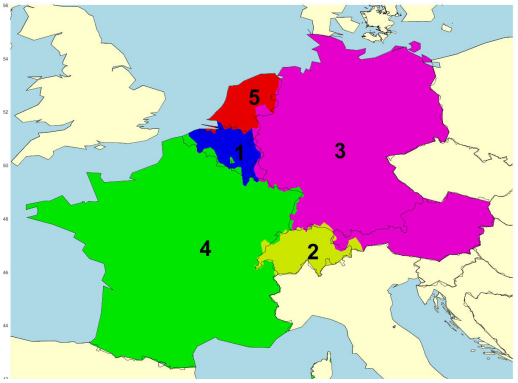

Figure 4: 5-ImpC.

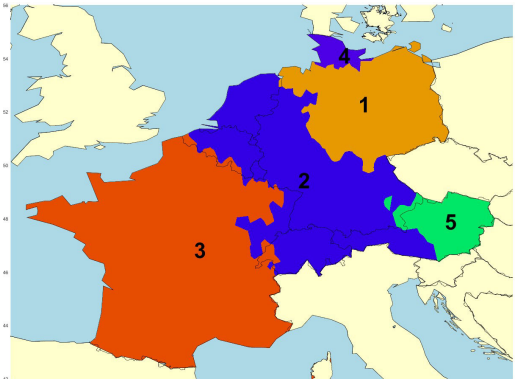

Figure 5: 8-ImpC.

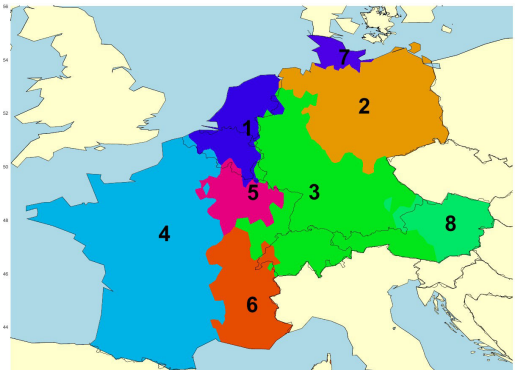

Figure 6: 14-ImpC.

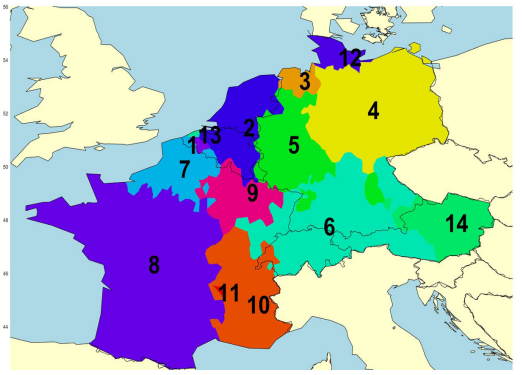

Figure 7: 28-ImpC.

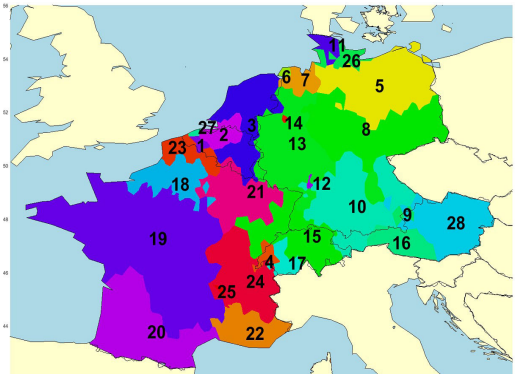

Figure 8: 50-ImpC.

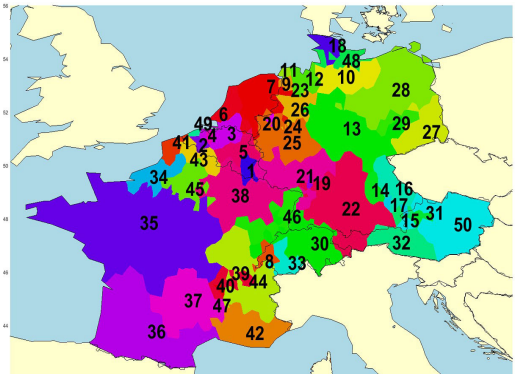

zones (dashed black line in Figure 9). This non-monotonicity is not straightforward. In short, the non-monotonic cost increase can be associated with three developments when increasing the number of PZs: First, an increase in the degrees of freedom of the EMCP; second, an increased number of LFCs, which—as explained in Felten et al. (2021)—are inaccurate in CWE-style zonal markets. Both developments are nonlinear and tend to impact MCC in opposite directions, which explains the

17. For colored illustrations please refer to the online version of the journal.

Figure 9: Differences of MCC, RDC and SC as well as CO_2 emissions compared to BAU-C.

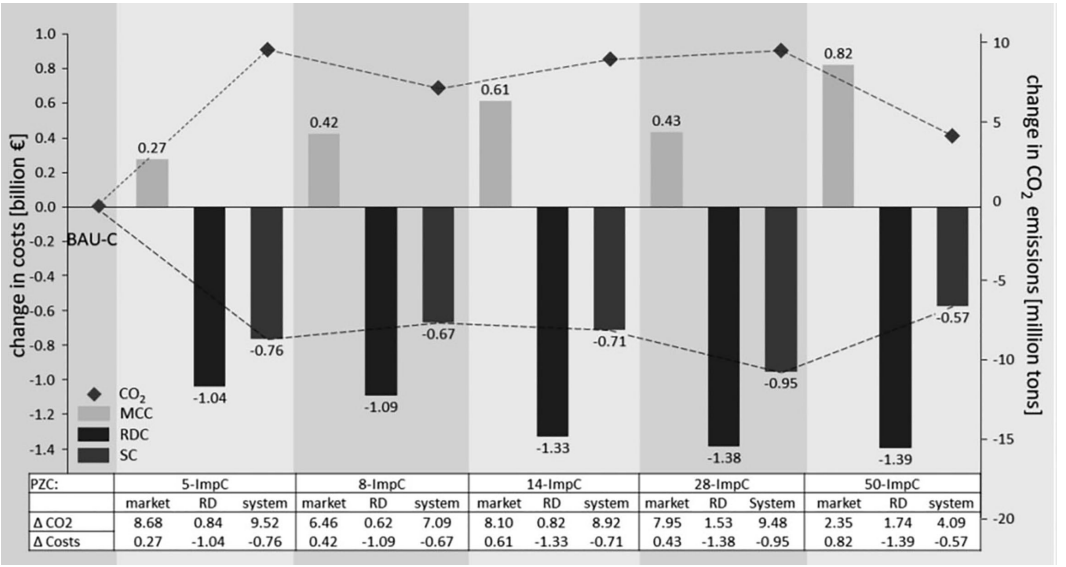

PZC:	5-ImpC			8-ImpC			14-ImpC			28-ImpC			50-ImpC		
	market	RD	system	market	RD	system	market	RD	system	market	RD	System	market	RD	system
Δ CO2	8.68	0.84	9.52	6.46	0.62	7.09	8.10	0.82	8.92	7.95	1.53	9.48	2.35	1.74	4.09
Δ Costs	0.27	-1.04	-0.76	0.42	-1.09	-0.67	0.61	-1.33	-0.71	0.43	-1.38	-0.95	0.82	-1.39	-0.57

non-monotonicity. For a very detailed analysis of these effects, the reader is referred to Appendix F.[18] Finally, as mentioned above, the clustering algorithm—while replicating the methodology of the first BZR—most likely does not identify optimal PZCs.

In terms of CO_2 emissions, all assessed improved PZCs lead to emission increases. However, this is not very surprising. In our case study (as well as in the European certificates market for the longest time), CO_2 prices are much below the level which would make electricity generation from hard coal and lignite be more expensive than gas-based generation. As MC is performed with the aim of welfare maximization, improved PZCs induce higher quantities of low-cost generation, even though the corresponding emissions are higher. However, this is a problem of pricing CO_2, not one of the investigated PZCs. As the highest SC decreases are achieved in the 28-ImpC, we focus our subsequent assessments on this configuration contrasting it with results of the BAU-C.

4.2.1 Market results

Figure 10 shows the yearly generation by fuel in CWE+ and selected (electrically) neighbouring countries for the BAU-C. The results correspond to the dispatch outcomes as determined by the market model JMM.

Figure 11 compares the generation in 28-ImpC to the BAU-C. It shows the corresponding differences in yearly electricity generation by fuel for the same countries as considered in Figure 10.

The main differences are linked to the creation of smaller zones in Northern Germany (cf. Figures 5 to 8). The split of the German PZ lets the market clearing consider LFCs inside Germany. These LFCs frequently become binding. The reason is that there is a surplus of electricity generation from wind farms in Northern Germany. Transmitting the complete surplus electricity to load centers elsewhere (mainly in the South) increases line loadings on these inner-German lines. Thus, these LFCs frequently induce market outcomes with reduced wind-based generation from these

18. Additionally, a direct comparison between the nodal pricing model and (simplified) FBMC is made in Felling (2021). There, nodal pricing serves as an upper benchmark and the author explains in which cases FBMC could come to the same results as the nodal pricing setup and which calibration, e.g. the introduction of FRMs, could prevent this.

Figure 10: Electricity generation by fuel for CWE and selected (electrically) neighbouring countries for the BAU-C[19]

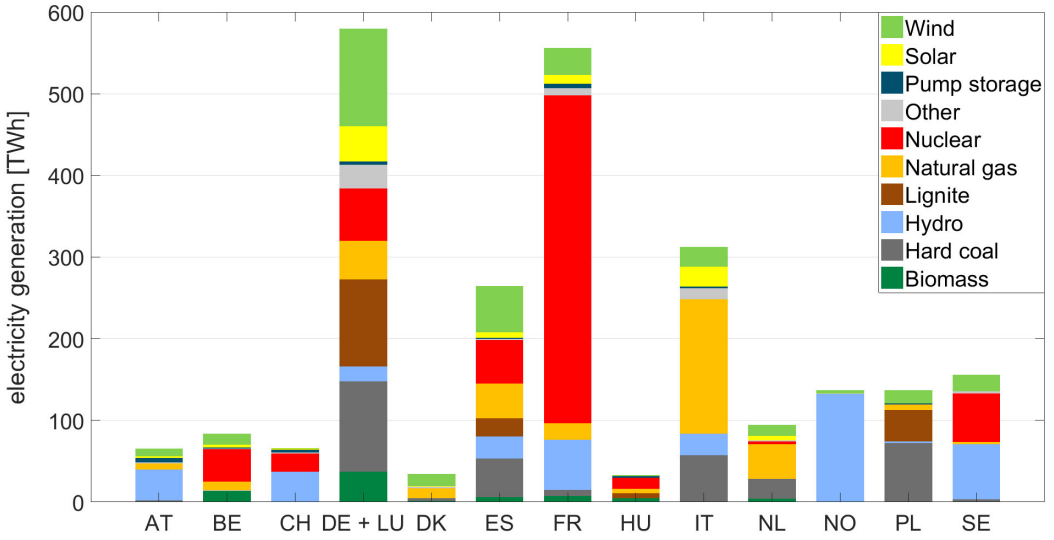

Figure 11: Change in electricity generation by fuel for CWE and selected (electrically) neighbouring countries (28-ImpC minus BAU-C)[20]

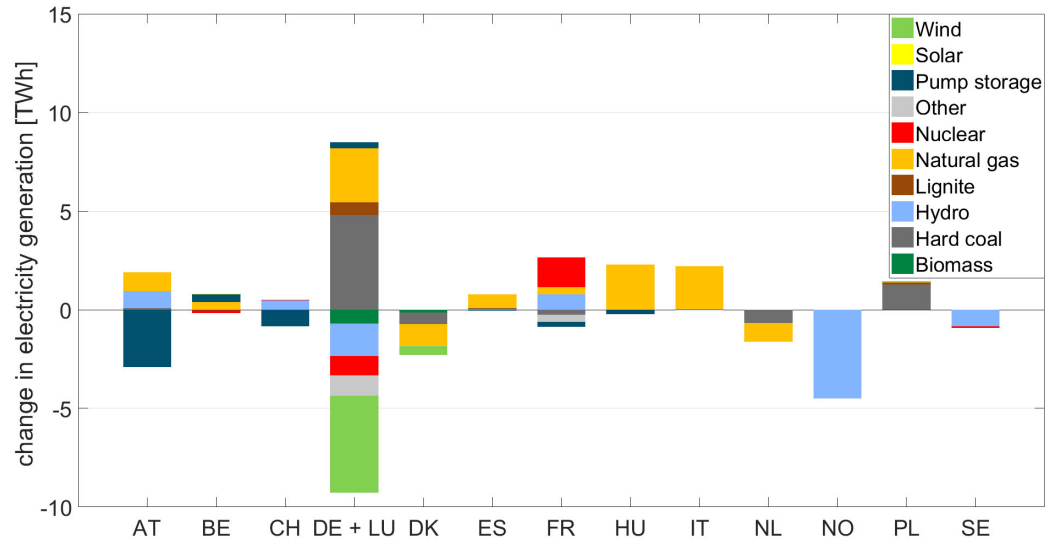

wind farms, due to limited transmission line capacities. Generation from wind in Germany therefore decreases by around 5 TWh in the 28-ImpC. Generation from wind in Denmark is affected in a similar way (i.e. a decrease of 0.5 TWh) albeit indirectly, as part of it would be transmitted through Northern Germany to the Southern regions. Similarly, Norwegian and Swedish generation from hydro reservoirs is reduced substantially (by around 5 TWh and 1 TWh respectively). These (and some other) generation reductions in the Nordic regions are mainly compensated by coal-based gen-

19. For colored illustrations please refer to the online version of the journal.
20. For colored illustrations please refer to the online version of the journal.

eration in Germany and Poland and by generation from natural gas in various Central and Southern European countries. Out of the latter group of countries, only the fossil-fuel-based generation of the Netherlands is reduced in the 28-ImpC. Considering these shifts in generation makes the increase of CO_2 emissions in the 28-ImpC become apparent. Finally, as the market clearing induces that less generation from wind in Northern Germany and Denmark is integrated, exchanges to the South are also reduced. Less varying wind-based generation is scheduled to be used in the Austrian PZ, and Austrian electricity prices become less volatile. This leads to a reduced use of pump storages in Austria (approx. 3 TWh less), as this technology exploits temporal price spreads.

Table 2 shows the average electricity prices for the BAU-C and 28-ImpC.[21] As the consideration of LFCs of inner-German lines has a major impact on generation, we also provide average prices for sub-regions of Germany (North/South). One can observe increases of electricity prices in Austria, Belgium, France and Southern Germany (PZs 8, 10 and 13, cf. Figure 7), a slight decrease in Switzerland and in the Netherlands as well as a strong decrease in Northern Germany.

Table 2: Average prices in CWE+ for the BAU-C and 28-ImpC.

prices [€/MWh]	AT	BE	CH	DE	DE-North [5-7,11,26]	DE-South [8,10,12-15]	FR	NL
BAU-C	27.5	28.7	30.0	27.5	27.5	27.5	27.5	31.3
28-ImpC	33.8	30.4	30.1	27.1	18.7	29.2	28.8	30.8

The smaller zones in Northern Germany (zones 6, 7, 11 and 26) even show average prices near or below zero. This plunge of prices is the consequence of a market clearing algorithm that includes transmission restrictions limiting low-cost generation in Northern Germany and in the Northern countries. If some of this generation is not eligible on the day-ahead market, a low-cost generator (e.g. a wind farm) will be the marginal generator which sets the electricity price in the corresponding PZ. In Germany, support schemes for generation from wind are in place; i.e. wind farm owners receive a market premium in addition to the wholesale market price for each unit of electricity generated. Thus, the marginal costs of generation from wind are even negative (in Germany) and so are the electricity prices if a wind farm is the marginal generator. In the BAU-C, wind farms do not become the marginal generator as the MC takes place as if there were no inner-German bottlenecks.[22] In terms of costs, free or very low-cost generation from wind, hydro and nuclear sources is replaced by more costly coal- and natural-gas-based generation. Hence, it is an obvious consequence that MCC increase by approx. 430 million € (cf. Figure 9).

Increased MCC are observed for all improved PZCs (cf. Figure 9). For 5-ImpC, the increase reaches 274 million € and, then, it varies between 420 and 820 million € for higher numbers of zones. This trend of increasing MCC can also be observed in Burstedde (2012). However, MCC changes reported in Burstedde (2012) are generally smaller and the increase is strictly monotonic. One explanatory factor for this is the difference in MC mechanisms used by Burstedde (2012) and by us. Instead of FBMC, Burstedde (2012) assumes an MC mechanism that considers an adjusted DC load flow without intra-zonal LFCs and aggregated nodes. Moreover, differences of input data and data aggregation (e.g. 79 aggregated grid nodes in Burstedde (2012)) are further explanatory factors. In addition to Burstedde (2012), our results can be contrasted with those of Neuhoff et al.

21. Where PZs and countries do not coincide, prices per country are calculated as the average prices of all assigned nodes, weighted by the yearly nodal demand. Thereby, the average price per node is equivalent to the average price of the corresponding zone.

22. Note that—physically—bottlenecks also exist in the BAU-C. However, they are only resolved at the redispatch stage (cf. Section 4.2.2).

(2013). Again, this paper is not 100% comparable to ours, as it uses NTC-based MC, considers a limited number of time steps, uses different data assumptions and only contrasts the BAU-C to nodal pricing—to name only few examples. However, Neuhoff et al. (2013) assess SC savings to range between 0.8 to 2.0 billion €. Our results are well within that range. In general, the increase of MCC with more PZs can be explained by the higher number of considered LFCs or, in the case of 5-ImpC, more relevant LFCs in the market clearing. In the BAU-C, the market clearing also considers LFCs of lines which are technically less critical (in terms of line overloads) and excludes others whose line loadings are critical more frequently. That is why, in the market clearing process, the use of low-cost generation in the BAU-C is not restricted to the same extent as it is in the improved configurations (which have been designed to consider the most critical lines in the MC). In principle, the impact is comparable to the previously mentioned case of market-driven wind curtailment in Northern Germany. As stated above, the MCC do not increase monotonically. We investigate this matter in detail in Appendix F.

4.2.2 Redispatch results

In Figure 9, we have shown that RDC are decreasing monotonically. In this section, we focus on the redispatch amounts being the main reason for this decrease. Annual amounts are presented in Table 3.

Table 3: Redispatch amounts and changes in line overloads relative to BAU-C

configuration	BAU-C	5	8	14	28	50
pos. redispatch [TWh]	21.3	8.2	6.3	3.3	1.9	1.8
change in overloads—inter-zonal [%]		+16	–29	–61	–81	–87
change in overloads—intra-zonal [%]		–79	–85	–93	–95	–97

For the 5-ImpC (i.e. same number of zones as in the BAU-C), the RDC decrease significantly (by 1.04 billion €). As stated in Section 2.7, the RDC vary with calibration of γ_u used in the redispatch assessment. In Appendix E, an approximation of effects is given. In particular, using $\gamma_u = 0$ could decrease the savings by around 200 million € for 28-ImpC. In turn, the choice of γ_u has only limited effect on redispatch quantities. The decreasing RDCs always go along with a substantial decrease in redispatch quantities (approx. 13 TWh). When the PZs are broken down further, the redispatch amounts and RDC continue to decrease. However, the absolute decrease of these values is much less than for the transition from the BAU-C to the 5-ImpC. E.g. from 28 to 50 zones, only decreases by approx. 10 million € and 0.1 TWh are achieved. The reason is that the main part of line overloads, especially on intra-zonal lines, is already avoided by the market clearing in 5-ImpC. Hence, PZs are delimited in a way that the most relevant, frequently congested lines run across zonal borders and, thus, congestion on these lines is managed more effectively. In 50-ImpC, even 97% of intra-zonal overloads (compared to the BAU-C) can be avoided. On inter-zonal lines, overloads even increase in 5-ImpC while decreasing thereafter.

Figure 12 illustrates the improvements between the BAU-C and 28-ImpC while Figure 13 confirms the observation of a diminishing marginal benefit with an increasing number of zones. Figure 12 presents the annual up- and down-ramping of plants and the scheduled line overloads as per market clearing. Triangles pointing upwards symbolize up-ramping, i.e. positive redispatch, triangles pointing downwards correspond to negative redispatch. The sizes of the triangles relate to the annual amounts of redispatch. The map on the left visualizes RD of the BAU-C while the right map in Figure 12 presents the results of the 28-ImpC. In addition, the numbers one to six in Figure

12 indicate the position of the six most overloaded lines in the BAU-C, which are also listed in Table 4. The colors of the lines indicate the cumulated line overloads as per market clearing throughout the year.

Figure 12: Redispatch amounts and yearly line overloading in BAU-C (left) and 28-ImpC (right)[23]

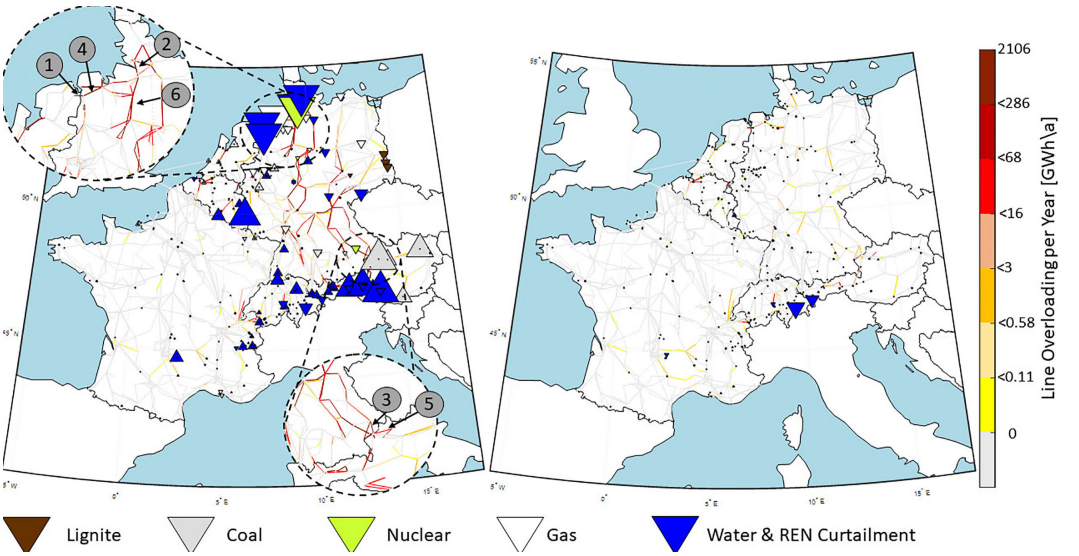

Table 4: Overview of most congested lines in BAU-C

line	connected locations	line overloading [GWh/a] in BAU-C	considered as LFC in
1	Diele-Meeden	2,108	BAU-C, All ImpC
2	Willster-Dollern	1,802	All ImpC
3	Pleitning-Pirach	1,695	All ImpC
4	Conneforde-Diele	1,399	50-ImpC
5	Pirach-St.Peter	1,337	28-ImpC,50-ImpC
6	Sottrum-Lande	1,184	28-ImpC,50-ImpC

In the BAU-C, most (scheduled) overloads occur in Northern Germany and at the border between Germany and Austria. Overloads on lines in Central Germany are less but still significant. In fact, four out of the six most congested lines are found in Northern Germany. The other two lines are located at the border to Austria. The details are shown in the zooming circles in Figure 12 and Table 4. These overloads cause the need for significant negative redispatch actions and curtailment of renewables in the North and North-East of Germany and positive redispatch in the Southern regions (mainly in Austria). The massive drop of redispatch, not only from the BAU-C to 28-ImpC but especially from the BAU-C to 5-ImpC, is achieved by considering the LFCs of the most congested lines in the market clearing process. Table 4 shows the configurations in which these lines are considered in the market clearing problem. The three most congested lines are explicitly considered in the 5-ImpC and are hence also present as LFCs in the other improved configurations (due to the hierarchical structure of the PZ clustering algorithm). The resulting effect is exhibited in Figure 13. It shows the relative changes in cumulated yearly (scheduled) line overloads compared to and nor-

23. For colored illustrations please refer to the online version of the journal.

malized by the overloads of the BAU-C. The line overloads of all six lines are reduced drastically (mostly, by more than 50% by the 5-ImpC and by more than 90% latest by the 28-ImpC). Notably, the transmission line "Diele-Meeden" runs across the border between Germany and the Netherlands and, thus, is already considered in the BAU-C. However, overloads can be reduced substantially by improved PZCs (e.g. already by 30% in the 5-ImpC). By introducing the new PZs in Northern Germany, zonal line load sensitivities for FBMC are more accurate. That is, in the BAU-C, the line loading impact of infeed of wind parks is dispersed in the whole net position of the German-Austrian PZ. The new Northern German PZs are relatively small and their zonal line load sensitivities yield loads closer to the actual line loads. In addition, the relief on "Diele-Meeden" in the 5-ImpC is also due to the consideration of the LFCs of the line "Wilster-Dollern" closeby. Another important line is "Pleitning-Pirach" which runs across the German-Austrian border and whose overloads are reduced by 62% and more.[24]

Figure 13: Reduced line overloading most congested lines in the BAU-C.

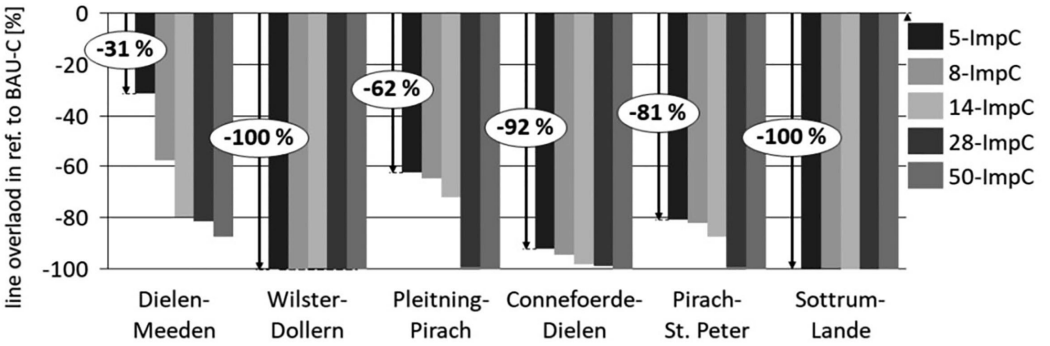

4.2.3 Distribution of welfare gains

Changes in MCC correspond to the negative sum of changes in consumer rents, congestion rents and producer rents. Figure 14 shows this segmentation along with RDC. RDC strongly decrease already for the 5-ImpC compared to the BAU-C and then marginal RDC changes converge against zero for an increasing number of zones (cf. Section 4.2). Hence the approximate selection of cost-minimizing price zone configurations (cf. Section 2.2) does at least guarantee that redispatch cost consistently decrease with increasing number of zones. For the market clearing cost and the related changes in rents, observations are yet less consistent. Congestion rents show the opposite behavior, i.e. increasing almost monotonically with the number of zones, but stabilizing at an increase of approx. 1,900 million € compared to the BAU-C. Consumer rents also rise with an increasing number of zones, except that they become lower for 28 zones than they are for 14 zones. Producer rents show the opposite behavior. Yet, their decrease is much stronger than the increase in consumer rents.

Additionally, changes between the 28-ImpC and the BAU-C at country level are shown in Table 5. Consumer rents drop in all CWE countries except Germany and the Netherlands and increase outside of CWE. This is directly related to the country-specific development of the base price (Table 2). The increases in congestion rents occur mostly in countries with a high number of significantly congested lines, i.e. in Germany and, to a lesser extent, in Belgium and France. Biggest changes in terms of producer rents occur in Germany, France and outside of CWE. In Germany and

24. Note that we have assumed a common German-Austrian PZ in the BAU-C.

Figure 14: Changes in rents and costs compared to BAU-C for all PZCs

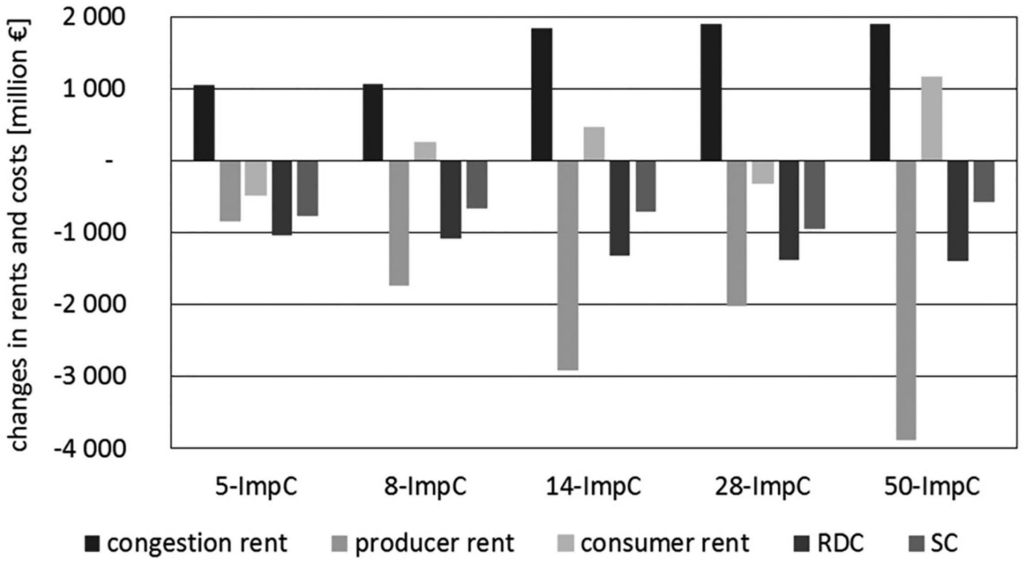

outside of CWE, producer rents drop, mainly because larger amounts of low-cost wind, nuclear (Germany) and hydro (Norway) energy are replaced by more expensive fuels or generation in other countries, while prices decrease at the same time. In France, both prices and generation increase, resulting in an increased producer rent. As a result, MCC (adjusted for value of imports and exports) increase mostly in Germany and decrease especially in the Netherlands.

With redispatch being reduced mostly in Germany and Austria, all CWE countries except Belgium benefit in total from the PZ reconfiguration. Biggest profiteers are the Netherlands, followed by Germany and France.

Table 5: Changes in rents/costs of 28-ImpC compared to BAU-C [million]

country	cons. rent	cong. rent	prod. rent	MCC	RDC	SC
AT	–419	102	300	16	–138	–122
BE	–139	241	–259	157	–21	136
CH	–48	95	–35	–11	–12	–23
DE	255	1,228	–2,298	815	–1,172	–357
FR	–691	193	692	–194	–7	–201
LU	–14	–16	52	–22	—	–22
NL	58	13	328	–399	–31	–430
CWE	–999	1,856	–1,220	362	–1,382	–1,020
Non-CWE	685	47	–800	68	—	68
System total	–314	1,903	–2,019	430	–1,382	–952

4.3 Results of sensitivity analyses

In Section 2.4, we have explained several sensitivity analyses. Figure 15 shows the differences in system costs (SC = MCC + RDC) contrasting the results of the sensitivity calculations with the corresponding PZC run of the reference case. Overall, our data show that the results of improved PZCs are quite robust against changes in the FBMC process. More precisely, the maximum SC difference occurs for 50-ImpC in the FRM sensitivity, being 103 million €. Compared to savings of

574 million € in the reference case, this variation is relatively small. In other words, re-classifying most congested intra-zonal lines and making them become inter-zonal has more leverage than all assessed sensitivities.

Figure 15: SC differences of the sensitivity calculations in comparison to the corresponding PZC reference case

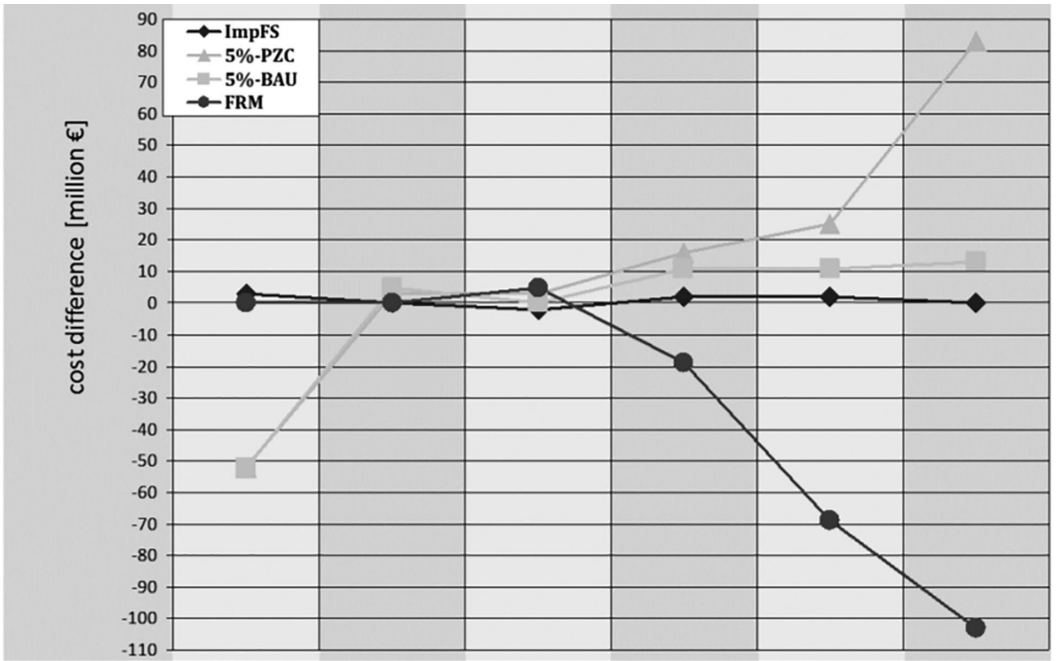

	BAU-C	5-ImpC	8-ImpC	14-ImpC	28-ImpC	50-ImpC
reference case	-	- 1 041	- 928	- 1 022	- 1 301	- 928

Calculating FBMC parameters based on renewable time series subject to forecast errors (ImpFS) has very little influence on system costs. This result is surprising at first sight. However, the direction of a forecast error of renewables can reinforce or relieve congestion. Thus, a random and limited error seems to have no structural effect on MC results. Considering intra-zonal lines as LFCs in the EMCP (5%-PZC and 5%-BAU) leads to lower SC for the BAU-C but to increased SC especially for 14-ImpC to 50-ImpC. Considering LFCs of very rarely congested intra-zonal lines in the EMCP—as is especially done when using the 5%-PZC for PZCs with 14 or more PZs—can only avoid little overloads. In turn, managing congestion of these lines is especially ineffective (cf. Felten et al. (2021). If these LFCs are inaccurate, it may cause welfare losses.[25] Thus, the cost-benefit ratio of including intra-zonal LFCs becomes worse with an increasing number of PZs. The FRM sensitivity has the largest effect on SC, as it substantially lowers MCC. For 8-ImpC, the FRM decrease results in higher redispatch amounts and costs, even exceeding the MCC decrease. Thus, the chosen FRM decrease is too high. However, for all other PZCs, the SC decrease significantly.

In addition to the assessed sensitivities and as mentioned in Section 1, the Clean Energy Package stipulates a fixed threshold on inter-zonal lines to be made available for cross-zonal trade. This threshold is to be increased from 20% in 2020 to 70% in 2025. The analysis of this change in regulation is out of the scope of this paper. However, Matthes et al. (2019) and Voswinkel et al.

25. This statement is substantiated by the detailed analysis in Appendix F.

(2019) show that this measure reduces market clearing costs. However, Voswinkel et al. (2019) also find that these so-called "Minimum RAMs" (MinRAMs) have adverse impacts on redispatch volumes and costs, impacting overall welfare (market clearing and redispatch) negatively.

5. CONCLUSION

Felten et al. (2021) derive analytically and based on a small-scale example several causes of inefficiencies in CWE-style FBMC. The paper at hand further addresses them, by presenting a novel large-scale model framework that enables the reproduction of FBMC to assess power systems undergoing structural changes. This framework is applied to assess improved PZCs in a zonal pricing regime using CWE-style FBMC. Our analysis has shown that very relevant welfare gains can be achieved by improved PZCs. Notably, redispatch amounts and associated costs can be reduced significantly. In the best PZC of this study, overall welfare can be increased by around 1 billion € (1.8% of the total system costs), redispatch amounts can be reduced by over 90%. Given the mentioned shortcomings of the clustering algorithm (cf. Section 4.2.1 as well as Felling (2021) and Ambrosius et al. (2020), these results have to be interpreted with care. One has to keep in mind that there might be PZCs with the same number of zones with better results. However, a similar algorithm was used to identify PZCs in the first and second BZR and, despite their potential sub-optimality, significant welfare gains can be achieved by reshaping PZCs.

Moreover, we have demonstrated that welfare gains are not equally distributed to market participants, which is likely to cause political frictions in the process of implementing improved PZCs. Furthermore, we have seen that the main driver for welfare gains is the improved congestion management of intra-zonal lines. Nonetheless, inaccuracies inherent to the FBMC procedures gain in importance when the number of price zones is increased, while simultaneously the relevance of intra-zonal congestion diminishes. These peculiarities of FBMC should already be considered in the process of PZC determination as investigated in Felling (2021).

ACKNOWLEDGMENTS

This research has partly been funded by the Federal Ministry for Economic Affairs and Energy (BMWi) of Germany within the framework of the joint project "KoNeMaSim—Kopplung von Netz- und Marktsimulationen für die Netzplanung" (project number 03ET7526). The authors gratefully acknowledge the financial support. We further thank conference and workshop participants at ÖGOR Workshop Vienna, the 40th and 41st IAEE International Conferences as well as Steven Gabriel, Benjamin Hobbs and William Hogan for valuable comments.

REFERENCES

50Hertz Transmission GmbH, Amprion GmbH, TenneT TSO GmbH, and TransnetBW GmbH (2014). Netzentwicklungsplan Strom 2014. URL https://www.netzentwicklungsplan.de/de/netzentwicklungsplaene/netzentwicklungsplaene-2024.

50Hertz Transmission GmbH, Amprion GmbH, TenneT TSO GmbH, and TransnetBW GmbH (2016). EEG-Anlagenstammdaten Gesamtdeutschland zur Jahresabrechnung 2015. URL https://www.netztransparenz.de/EEG/Anlagenstammdaten.

50Hertz Transmission GmbH, Amprion GmbH, TenneT TSO GmbH, and TransnetBW GmbH (2018). Szenariorahmen für den Netzentwicklungsplan Strom 2030 (Version 2019). URL https://www.netzentwicklungsplan.de/de/netzentwicklungsplaene/netzentwicklungsplan-2030-2019.

ACER (Agency for the Cooperation of Energy Regulators) (2020). Public consultation on the methodology and assumptions that are to be used in the bidding zone review process and for the alternative bidding zone configurations to be considered. URL https://www.acer.europa.eu/Official_documents/Public_consultations/Pages/PC_2020_E_08.aspx.

ACER (Agency for the Cooperation of Energy Regulators) (2014). Report on the influences of existing bidding zones on electricity markets. URL http://www.acer.europa.eu/official_documents/acts_of_the_agency/publication/acer

Ambrosius, M., V. Grimm, T. Kleinert, F. Liers, M. Schmidt, and G. Zöttl (2020). "Endogenous price zones and investment incentives in electricity markets: An application of multilevel optimization with graph partitioning." *Energy Economics* 92. https://doi.org/10.1016/j.eneco.2020.104879.

Amprion GmbH, 50Hertz Transmission GmbH, TenneT TSO GmbH, and TransnetBW GmbH (2019). Abschlussbericht systemanalysen 2019. URL https://www.bundesnetzagentur.de/SharedDocs/Downloads/DE/Sachgebiete/Energie/Unternehmen_Institutionen/Versorgungssicherheit/Berichte_Fallanalysen/Systemanalyse_UeNB_2019.pdf?__blob=publicationFile v=5.

Amprion GmbH, APX, Belpex, Creos, Elia System Operator S.A, EpexSpot, T. Réseau de transport d'électricité (RTE), and TransnetBW GmbH (2014). Documentation of the CWE FB MC solution as basis for the formal approval-request. URL https://www.bundesnetzagentur.de/DE/Sachgebiete/ElektrizitaetundGas/Unternehmen_Institutionen/Netzzugang_Messwesen/Marktkopplung_Strom/Marktkopplung-node.html.

Androcec, I. and S. Krajcar (2012). "Methodology of market coupling/splitting for efficient cross-border electricity trading." In *2012 9th International Conference on the European Energy Market*, pages 1–8. https://doi.org/10.1109/EEM.2012.6254650.

APG (Austrian Power Grid AG) (2017). Leitungsnetz. URL https://www.apg.at/de/netz/anlagen/leitungsnetz.

Autoriteit Consument & Markt (ACM), Bundesnetzagentur (BNetzA), Commission de Régulation de l'énergie (CRE), Commission de Régulation de l'électircité et du Gaz (CREG), E-Control, and ILR (2015). Position paper of CWE NRAs on flow-based market coupling. URL http://www.creg.info/pdf/Opinions/2015/b1410/CWE_NRA_Position_Paper.pdf.

BDEW Bundesverband der Energie- und Wasserwirtschaft e.V. Redispatch in Deutschland—Auswertung und Transparenzdaten, 2017. URL https://www.bdew.de/service/anwendungshilfen/redispatch-deutschland/.

Bertsch, J., S. Hagspiel, and L. Just (2016). Congestion management in power systems. *Journal of Regulatory Economics* 500(3): 290–327. ISSN 1573-0468. https://doi.org/10.1007/s11149-016-9310-x.

Biggar, D.R. and M.R. Hesamzadeh (2014). *The economics of electricity markets*. Wiley—IEEE, 1st edition. ISBN 9781118775752. https://doi.org/10.1002/9781118775745.

Bjørndal, M. and K. Jörnsten (2001). "Zonal pricing in a deregulated electricity market." *The Energy Journal* 22(3): 51–73. https://doi.org/10.5547/ISSN0195-6574-EJ-Vol22-No1-3.

Bjørndal, M. and K. Jörnsten (2007). "Benefits from coordinating congestion management—the Nordic power market." *Energy policy* 350(3): 1978–1991. https://doi.org/10.1016/j.enpol.2006.06.014.

Bjørndal, M., K. Jørnsten, and V. Pignon (2003). "Congestion management in the nordic power market—counter purchase and zonal pricing." *Journal of Network Industries* 40(3): 271–291. https://doi.org/10.1177/178359170300400302.

Breuer, C. (2014). *Optimale Marktgebietszuschnitte und ihre Bewertung im europäischen Stromhandel*. PhD thesis.

Bundesamt für Statistik (2015). Bruttowertschöpfung (bws) nach kanton und aktivitäten, 2015. URL https://www.bfs.admin.ch/bfs/de/home/aktuell/covid-19.assetdetail.19544490.html.

BNetzA (Bundesnetzagentur für Elektrizität, Gas, Telekommunikation, Post und Eisenbahnen) (2018). Kraftwerksliste. URL https://www.bundesnetzagentur.de/DE/Sachgebiete/ElektrizitaetundGas/Unternehmen_Institutionen/Versorgungssicherheit/Erzeugungskapazitaeten/Kraftwerksliste/kraftwerksliste-node.html.

BNetzA (Bundesnetzagentur für Elektrizität, Gas, Telekommunikation, Post und Eisenbahnen) and Bundeskartellamt (2018). Monitoringbericht 2018. URL https://www.bundesnetzagentur.de/DE/Sachgebiete/ElektrizitaetundGas/Unternehmen_Institutionen/DatenaustauschundMonitoring/Monitoring/Monitoringberichte/Monitoring_Berichte_node.html.

Burstedde, B. (2012). "From nodal to zonal pricing: A bottom-up approach to the second-best." In *European Energy Market (EEM), 2012 9th International Conference on the*, pages 1–8. IEEE. https://doi.org/10.1109/EEM.2012.6254665.

Deutscher Wetterdienst (2017). *Regional Model COSMO-EU*. URL https://www.dwd.de/EN/research/weatherforecasting/num_modelling/01_num_weather_prediction_modells/regional_model_cosmo_eu.html.

Dierstein, C. (2017). "Impact of generation shift key determination on flow based market coupling." *14th International Conference on the European Energy Market (EEM), Dresden*. https://doi.org/10.1109/EEM.2017.7981901.

Egerer, J., J. Weibenzahn, and H. Hermann (2015). "Two price zones for the german electricity market: Market implications and distributional effects." URL https://www.diw.de/sixcms/detail.php?id=diw_01.c.497248.de. https://doi.org/10.2139/ssrn.2568647.

Ehrenmann, A. and Y. Smeers (2005). "Inefficiencies in European congestion management proposals." *Utilities policy* 130(2): 135–152. https://doi.org/10.1016/j.jup.2004.12.007.

Elia System Operator S.A. (2015). URL http://www.elia.be/en/grid-data/.

Elia System Operator S.A. (2016). Solar-pv/wind power generation data. URL https://www.elia.be/en/grid-data/power-generation.

Energate GmbH (2018). Marktdaten. URL http://www.energate-messenger.de/markt/.

Energienetze Offenbach (2013). Summenlast der nicht leistungsgemessenen kunden 2012. URL https://www.energienetze-offenbach.de/veroeffentlichungen.

European Network of Transmission System Operators for Electricity Entso-E (2015). Scenario outlook and adequacy forecast. URL https://docs.entsoe.eu/dataset/scenario-outlook-adequacy-forecast-so-af-2015.

Entso-E (European Network of Transmission System Operators for Electricity) (2014). Ten year network development plan (tyndp).

Entso-E (European Network of Transmission System Operators for Electricity) (2015). Hourly load values for all countries. URL https://www.entsoe.eu/db-query/consumption/mhlv-all-countries-for-a-specific-month.

Entso-E (European Network of Transmission System Operators for Electricity) (2016a). Specific national considerations. URL https://www.entsoe.eu/publications/statistics-and-data/.

Entso-E (European Network of Transmission System Operators for Electricity) (2018a). First edition of the bidding zone review—final report. URL https://eepublicdownloads.entsoe.eu/clean-documents/nc-tasks/EBGL/CACM_A32_2018-03_First_Edition_of_the_Bidding_Zone_Review

Entso-E (European Network of Transmission System Operators for Electricity) (2018b). Transparency platform. URL https://transparency.entsoe.eu/.

EurObserv'ER (2013a). Photovoltaic barometer 2013. URL https://www.eurobserv-er.org/pdf/photovoltaic-barometer-2013-fr-en/.

EurObserv'ER (2013b). Wind energy barometer 2013. URL https://www.eurobserv-er.org/pdf/wind-energy-barometer-2013-fr-en/.

EurObserv'ER (2014a). Photovoltaic barometer 2014. URL https://www.eurobserv-er.org/pdf/photovoltaic-barometer-2014-en/.

EurObserv'ER (2014b). Wind energy barometer 2014. URL https://www.eurobserv-er.org/pdf/wind-energy-barometer-2014-en/.

European Commission (2015). Commission Regulation (EU) 2015/1222 of 24 July 2015 establishing a guideline on capacity allocation and congestion management URL https://eur-lex.europa.eu/legal-content/DE/TXT/?uri=CELEX

Eurostat (2015a). Area by nuts 3 region. URL http://appsso.eurostat.ec.europa.eu/nui/show.do?dataset=reg_area3 lang=en.

Eurostat (2015b). Gross value added at basic prices by nuts 3 regions. URL http://ec.europa.eu/eurostat/web/products-datasets/-/nama_10r_3gva.

Eurostat (2015c). Population on 1 january by broad age group, sex and nuts 3 region. URL https://appsso.eurostat.ec.europa.eu/nui/show.do?dataset=demo_r_pjanaggr3 lang=en.

EVNG (2013). Summenlast der nicht leistungsgemessenen kunden im gj 2012 URL https://www.evng.de/netzrelevante-daten.html.

Felling T. (2019). "Solving the bi-level problem of a closed optimization of electricity price zone configurations using a genetic algorithm." *HEMF Working Paper*, 9. URL http://www.sciencedirect.com/science/article/pii/S0301421519306482. http://doi.org/10.2139/ssrn.3425831.

Felling, T. (2021). "Development of a genetic algorithm and its application to a bi-level problem of system cost optimal electricity price zone configurations." *Energy Economics* 101. https://doi.org/10.1016/j.eneco.2021.105422.

Felling, T. and C. Weber (2018). "Consistent and robust delimitation of price zones under uncertainty with an application to Central Western Europe." *Energy Economics* 75: 583–601. https://doi.org/10.1016/j.eneco.2018.09.012.

Felten, B. (2020). "An integrated model of coupled heat and power sectors for large-scale energy system analyses." *Applied Energy*, 266: 114521. ISSN 0306-2619. URL http://www.sciencedirect.com/science/article/pii/S0306261920300337. https://doi.org/10.1016/j.apenergy.2020.114521.

Felten, B., P. Osinski, T. Felling, and C. Weber (2021). "The flow-based market coupling domain—why we can't get it right." *Utilities Policy* 70: 101136. https://doi.org/10.1016/j.jup.2020.101136.

Finck, R., A. Ardone, and W. Fichtner (2018). "Impact of flow-based market coupling on generator dispatch in cee region." In *2018 15th International Conference on the European Energy Market (EEM)*, pages 1-5. IEEE, Piscataway, New Jersey. ISBN 978-1-5386-1488-4. https://doi.org/10.1109/EEM.2018.8469927.

Grimm, V., A. Martin, M. Weibelzahl, and G. Zöttl (2016). "On the long run effects of market splitting: Why more price zones might decrease welfare." *Energy Policy* 94: 453–467. ISSN 0301-4215. https://doi.org/10.1016/j.enpol.2015.11.010.

Grimm, V. et al. (2016). "Transmission and generation investment in electricity markets: The effects of market splitting and network fee regimes." *European Journal of Operational Research* 2540(2): 493–509. https://doi.org/10.1016/j.ejor.2016.03.044.

Grimm, V., T. Kleinert, F. Liers, M. Schmidt, and G. Zöttl (2019). "Optimal price zones of electricity markets: a mixed-integer multilevel model and global solution approaches." *Optimization Methods and Software* 340(2): 406–436. https://doi.org/10.1080/10556788.2017.1401069.

Grimm, V., B. Rückel, C. Sölch, and G. Zöttl (2021). "The impact of market design on transmission and generation investment in electricity markets." *Energy Economics* 93. https://doi.org/10.1016/j.eneco.2020.104934.

Hogan, W.W. (1992). "Contract networks for electric power transmission." *Journal of Regulatory Economics* 40(3): 211–242. https://doi.org/10.1007/BF00133621.

Imran, M. et al. (2008). "Effectiveness of zonal congestion management in the European electricity market." In *Power and Energy Conference, 2008. PECon 2008. IEEE 2nd International*, pages 7–12. https://doi.org/10.1109/PECON.2008.4762432.

IEA (International Energy Agency) (2014). IEA electricity information.

Kłos. M. et al. (2014). "The scheme of a novel methodology for zonal division based on power transfer distribution factors." In *IECON 2014—40th Annual Conference of the IEEE Industrial Electronics Society*, pages 3598–3604. https://doi.org/10.1109/IECON.2014.7049033.

Lang, L.M., B. Dallinger, and G. Lettner (2020). "The meaning of flow-based market coupling on redispatch measures in Austria." *Energy Policy* 136: 111061. ISSN 0301-4215. URL http://www.sciencedirect.com/science/article/pii/S0301421519306482. https://doi.org/10.1016/j.enpol.2019.111061.

Löschel, A., F. Flues, F. Pothen, and P. Massier (2013). Den Strommarkt an die Wirklichkeit anpassen: Skizze einer neuen Marktordnung. URL https://www.zew.de/de/publikationen/den-strommarkt-an-die-wirklichkeit-anpassen-skizze-einer-neuen-marktordnung-1/?cHash=c8dee7ba2f6cbe07666709c4564434bf.

Marjanovic, I., D. v. Stein, N. van Bracht, and A. Moser (2018). "Impact of an enlargement of the flow based region in continental Europe." In *2018 15th International Conference on the European Energy Market (EEM)*, pages 1–5. https://doi.org/10.1109/EEM.2018.8470008.

Matthes, B., C. Spieker, D. Klein, and C. Rehtanz (2019). "Impact of a minimum remaining available margin adjustment in flow-based market coupling." In *2019 IEEE Milan PowerTech*, pages 1–6. https://doi.org/10.1109/PTC.2019.8810504.

Meibom, P., H. V. Larsen, R. Barth, H. Brand, C. Weber, and O. Woll (2006). "Wilmar joint market model. Documentation." Technical report, Risø National Laboratory. URL https://orbit.dtu.dk/en/publications/wilmar-joint-market-model-documentation(537d7680-a413-4a82-9e69-e1943cdface7).html.

Meibom, P. et al. (2011). "Stochastic optimization model to study the operational impacts of high wind penetrations in Ireland." *IEEE Transactions on Power Systems* 260(3): 1367–1379. ISSN 0885-8950. https://doi.org/10.1109/TPWRS.2010.2070848.

Ministère de la Transition Ecologique. Installations photovoltaïques/éoliennes raccordées au réseau: résultats par département et région, 2015. URL http://www.statistiques.developpement-durable.gouv.fr/energie-climat.

MVV Netze (2013). Summenlast der nicht leistungsgemessenen kunden 2012. URL https://www.mvv-netze.de/unternehmen/veroeffentlichungspflichten.

Neuhoff, K. et al. (2013). "Renewable electric energy integration: quantifying the value of design of markets for international transmission capacity." *Energy Economics* 40: 760–772. https://doi.org/10.1016/j.eneco.2013.09.004.

Nielsen, M. et al. (2016). "Economic valuation of heat pumps and electric boilers in the Danish energy system." *Applied Energy* 167: 189–200. ISSN 0306-2619. https://doi.org/10.1016/j.apenergy.2015.08.115.

Oberlandesgericht Düsseldorf (OLG) (2015). Beschluss VI-3 Kart 313/12 (V) vom 28.4.2015. https://doi.org/10.7328/jurpcb20153013.

Oggioni, G. and Y. Smeers (2013). "Market failures of market coupling and counter-trading in Europe: An illustrative model based discussion." *Energy Economics* 35: 74–87. https://doi.org/10.1016/j.eneco.2011.11.018.

Open Power System Data (2019). Time series package version 2019-06-05. URL https://data.open-power-system-data.org/time_series/2019-06-05.

Osinski, P., R. Becker, and C. Weber (2016). *Regional modelling of electric load and renewable infeed time series in Europe*.

Ovaere, M., J. Bellenbaum, F. M. Baldursson, S. Proost, C. Weber, G. Kjolle, and E. Lazarczyk (2016). *Garpurr d3.1, quantification method in the absence of market response and with market response taken into account*.

Rijksoverheid (Government of the Netherlands) (2015). Regionale klimaatmonitor. URL https://klimaatmonitor.databank.nl/.

RTE (Réseau de Transport d'Electricité) (2015). Static grid model. URL https://clients.rte-france.com/lang/an/visiteurs/vie/indispos_caracteristiques_statiques.jsp.

S & P Global Platts (2018). World electric power plants database. URL https://www.platts.com/products/world-electric-power-plants-database.

Sarfati, M. et al. (2015). "Five indicators for assessing bidding area configurations in zonally-priced power markets." In *2015 IEEE Power Energy Society General Meeting*, pages 1–5. https://doi.org/10.1109/PESGM.2015.7286517.

Schönheit, D., R. Weinhold, and C. Dierstein (2020). "The impact of different strategies for generation shift keys (gsks) on the flow-based market coupling domain: A model-based analysis of central western Europe." *Applied Energy* 258: 114067. ISSN 0306-2619. URL http://www.sciencedirect.com/science/article/pii/S0306261919317544. https://doi.org/10.1016/j.apenergy.2019.114067.

Spiecker, S., P. Vogel, and C. Weber (2013). "Evaluating interconnector investments in the north European electricity system considering fluctuating wind power penetration." *Energy Economics* 37(1). https://doi.org/10.1016/j.eneco.2013.01.012.

Stadtwerke Landshut (2013). Summenlast der nicht leistungsgemessenen kunden 2012. URL https://www.stadtwerke-landshut.de/netze/.

Statistik Austria (2013). Bundesländer-energiebilanzen. URL http://www.statistik.at/web_de/statistiken/energie_umwelt_innovation_mobilitaet/energie_und_umwelt/energie/energiebilanzen/index.html.

Steffen, B. and C. Weber (2016). "Optimal operation of pumped-hydro storage plants with continuous time-varying power prices." *European Journal of Operational Research* 2520(1): 308–321. ISSN 0377-2217. https://doi.org/10.1016/j.ejor.2016.01.005.

Stromnetz Berlin (2013). Summenlast der nicht leistungsgemessenen kunden 2012. URL https://www.stromnetz.berlin/uber-uns/veroffentlichungspflichten/energiewirtschaftsgesetz-enwg.

TenneT TSO GmbH (2015). Static grid model. URL https://www.tennettso.de/site/en/Transparency/publications/static-grid-model/static-grid-model.

The Wind Power (2014). Europe wind farms database. URL https://www.thewindpower.net/store_continent_en.php?id_zone=1001.

Trepper, K., M. Bucksteeg, and C. Weber (2015). "Market splitting in Germany—new evidence from a three-stage numerical model of Europe." *Energy Policy* 87: 199–215. ISSN 03014215. https://doi.org/10.1016/j.enpol.2015.08.016.

Tuohy, A. et al. (2009). "Unit commitment for systems with significant wind penetration." *IEEE Transactions on Power Systems* 240(2): 592–601. ISSN 0885-8950. https://doi.org/10.1109/TPWRS.2009.2016470.

Van den Bergh, K. et al. (2016). "The impact of bidding zone configurations on electricity market outcomes." In *2016 IEEE International Energy Conference (ENERGYCON)*, pages 1–6. https://doi.org/10.1109/ENERGYCON.2016.7514031.

Varmelast (2018). Heating plans. URL https://www.varmelast.dk/en/heating-plans.

Voswinkel, S., B. Felten, T. Felling, and C. Weber (2019). "What drives welfare in Europe's approach to electricity market coupling?" Preprint. URL https://ssrn.com/abstract=3424708.

VREG (2015). URL http://www.vreg.be/nl/groene-stroom.

Weber, C. et al. (2009). *WILMAR—a stochastic programming tool to analyse the large scale integration of wind energy*. J. Kallrath, P. Pandalos, S. Rebenack, and M. Scheidt. https://doi.org/10.1007/978-3-540-88965-6_19.

Wyrwoll, L., K. Kollenda, C. Müller, and A. Schnettler (2018). "Impact of flow-based market coupling parameters on European electricity markets." In *2018 53rd International Universities Power Engineering Conference (UPEC)*, pages 1–6. https://doi.org/10.1109/UPEC.2018.8541904.

Zimmermann, R. and C. Murillo-Sánchez (2018). *Matpower User's Manual Version 7.0b1*. Power System Engineering Research Center. URL http://www.pserc.cornell.edu/matpower/.

Zimmermann, R., C. Murillo-Sánchez, and R. Thomas. "Matpower: Steady-state operations, planning and analysis tools for power system research and education." *IEEE Transactions on Power Systems* 260(1): 12–19. https://doi.org/10.1109/TPWRS.2010.2051168.

APPENDIX A. ABBREVIATIONS AND SYMBOLS

List of Abbreviations

BAU-C business-as-usual configuration.
CHP combined heat and power.
CWE(+) (extended) Central Western Europe(an).
DSO distributions system operator.
EMCP electricity market clearing problem.
FB(MC) flow-based (market coupling).
FRM flow reliability margin.
GSK Generation Shift Key
GVA gross value added.
ImpFS imperfect foresight. Sensitivity as explained in Section 2.4.
JMM WILMAR Joint Market Model.
LFC load flow constraint.
LMP locational marginal price.
MC market coupling.
MCC market clearing costs.
OPF optimal power flow.
PTDF power transfer distribution factor.
PZ(C) price zone (configuration).
RAM remaining available margin.
RDC redispatch costs.
SC system costs.
TSO transmission system operator.

Nomenclature

$A_{f,i}$	PTDF of line f for node i.
$b_{u,i}$	unit-to-node allocation.
c^{curt}	compensation for renewables curtailment.
C_f	capacity of line f.
c_t^{max}	variable costs of the most expensive power plant in the system at time t.
γ_u	factor as explained in Section 2.6.
$c_{u,t}$	variable costs of power plant u.
$c_{u,t}^{+/-}$	additional (avoided) costs for positive (negative) redispatch of unit u.
$\Delta C_{u,t}$	gap to absolute operational costs at full load.
$\Delta g_{u,t}$	gap to full load generation.
$\Delta g_{u,t}^{+/-}$	positive/negative redispatch of unit u at time t.
$\Delta g_{i,t}^{mbc}$	market-based renewables curtailment at node i.
$d_{i,t}$	vertical load at node i.
δ_u	power-loss coefficient of unit u ($\delta_u \geq 0$ *for* $u \in \mathcal{U}^{ext}$, 0 *otherwise*)
η_u^{ps}	cycle efficiency of pumped storage unit u.
$g_{u,t}$	scheduled dispatch of unit u.

$g_{u,t}^{max}$	available electric capacity of unit u.
$g_{u,t}^{nonsp,+}$	capacity reserved for positive nonspinning reserve.
$g_{u,t}^{spin,+}$	capacity reserved for positive spinning reserve.
$g_{u,t}^{spin,-}$	capacity reserved for negative spinning reserve.
$g_{u,t}^{started}$	started capacity of unit u.
$h_{u,t}^{chp}$	heat extraction of unit u ($h_{u,t}^{chp} \geq 0$ *for* $u \in \left\{\mathcal{U}^{ext} \cup \mathcal{U}^{bkp}\right\}$, 0 *otherwise*)
$i \in I$	index/set of nodes of the system.
κ_u	minimum load fraction of unit u.
$\mu_{u,t}^{hyr}$	shadow price of hydro reservoir unit u.
$^{ps}_{u,t}$	daily average electricity price (applicable in PZ of unit u).
q_i^{RD}	net electricity surplus at node i after redispatch.
σ_u	power-to-heat ratio of unit $u \in \left\{\mathcal{U}^{bkp} \cup \mathcal{U}^{ext}\right\}$.
τ_u^{lead}	lead time of unit u.
$\mathcal{U}^{bkp} \subset \mathcal{U}^{disp}$	set of backpressure CHP plants.
$\mathcal{U}^{conv}$	$= \mathcal{U} \setminus \mathcal{U}^{RES,nondisp}$
$\mathcal{U}^{disp}$	set of dispatchable generation units.
$\mathcal{U}^{ext} \subset \mathcal{U}^{disp}$	set of extraction-condensing CHP plants.
$\mathcal{U}^{hydro}$	$= \mathcal{U}^{ps,pump} \cup \mathcal{U}^{hyr}$
$\mathcal{U}^{hyr} \subset \mathcal{U}^{disp}$	set of hydro power plant with reservoirs.
$\mathcal{U}_t^{nonop}$	$= \left\{u \mid u \in \mathcal{U}^{disp} \wedge g_{u,t} = 0\right\}$
$\mathcal{U}_t^{noRD,pos}$	$= \mathcal{U} \setminus \mathcal{U}^{RD,pos}$
$\mathcal{U}_t^{noRD,neg}$	$= \mathcal{U} \setminus \mathcal{U}^{RD,neg}$
$\mathcal{U}^{ps,pump} \not\subset \mathcal{U}^{disp}$	set of pumps of pumped storage units.
$\mathcal{U}^{ps,turb} \subset \mathcal{U}^{disp}$	set of turbines of pumped storage units.
$\mathcal{U}^{RD,fast}$	$= \left\{u \mid u \in \mathcal{U}^{disp} \wedge \tau_u^{lead} \leq 1\right\} \setminus \mathcal{U}^{bkp}$
$\mathcal{U}_t^{RD,pos}$	$= \mathcal{U}_t^{started} \cup \mathcal{U}^{RD,fast}$
$\mathcal{U}_t^{RD,neg}$	$= \mathcal{U}_t^{started} \setminus \mathcal{U}^{bkp}$
$\mathcal{U}_t^{RD,slow}$	$= \mathcal{U}_t^{started} \setminus \mathcal{U}^{RD,fast} \setminus \mathcal{U}^{bkp}$
$\mathcal{U}^{RES,nondisp}$	set of renewable non-dispatchable units.
$\mathcal{U}_t^{started}$	$= \left\{u \mid u \in \mathcal{U}^{disp} \wedge g_{u,t} > 0\right\}$
$V^{(within)}$	price variation in system (if with superscript "within": Within-zone price variation).
$z \in Z$	index/set of price zones.

APPENDIX B. MODEL CHAIN

Figure 16 shows a flow chart of the complete model chain used in this study. It is divided into the following parts:

- (1): regional wind and renewable time series are created.
- between (1) and (2): vertical load on a nodal level is computed and aggregated to a zonal level depending on the node-to-zone allocation.
- (2): capacity allocation—starting point is the computation of PTDFs. Subsequently, the base case is computed, followed by the calculation of FBMC parameters (GSKs, zonal PTDFs).
- (3): FBMC parameters serve as input data for the market model JMM.
- (4): The dispatch and market results are handed over to the redispatch model.

Figure 16: Flow chart of the developed model framework, sketching a typical FBMC assessment (D-2 to D stage).

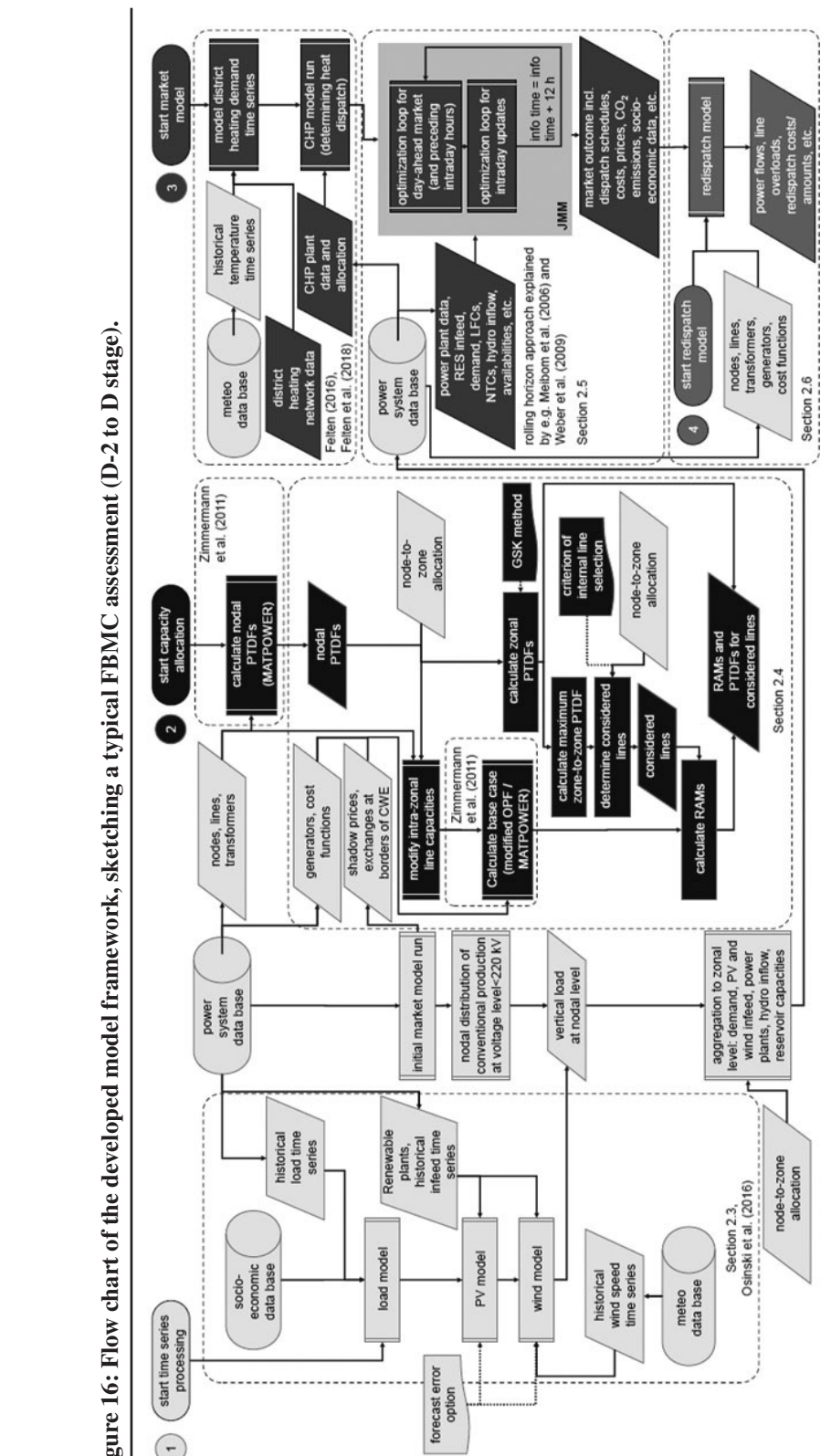

APPENDIX C. REGIONAL RENEWABLE AND LOAD MODELLING

Figure 17: Flow chart of the model for regional load time series

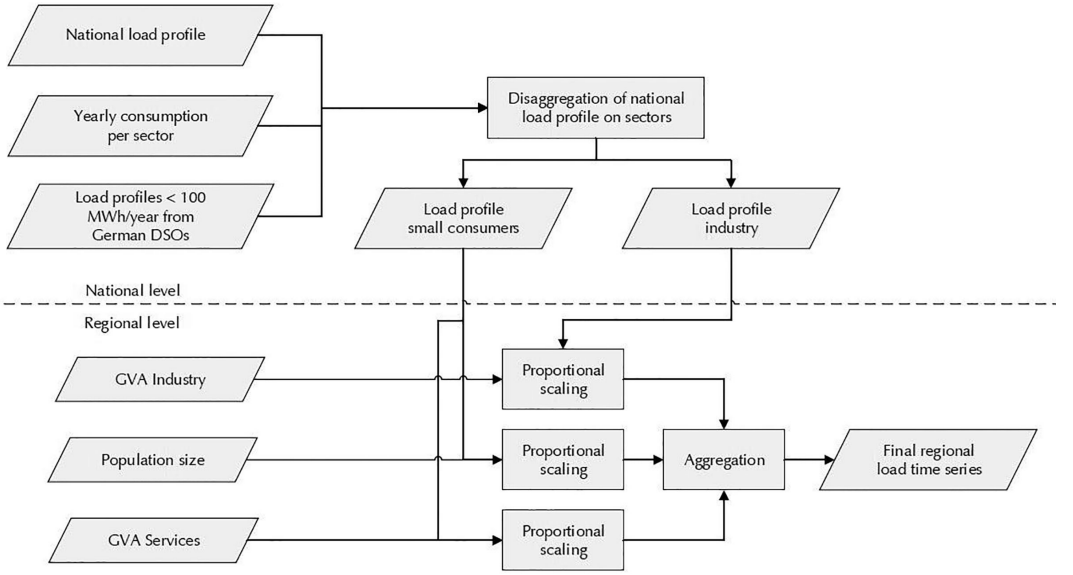

Figure 18: Flow chart of the model for regional renewable time series

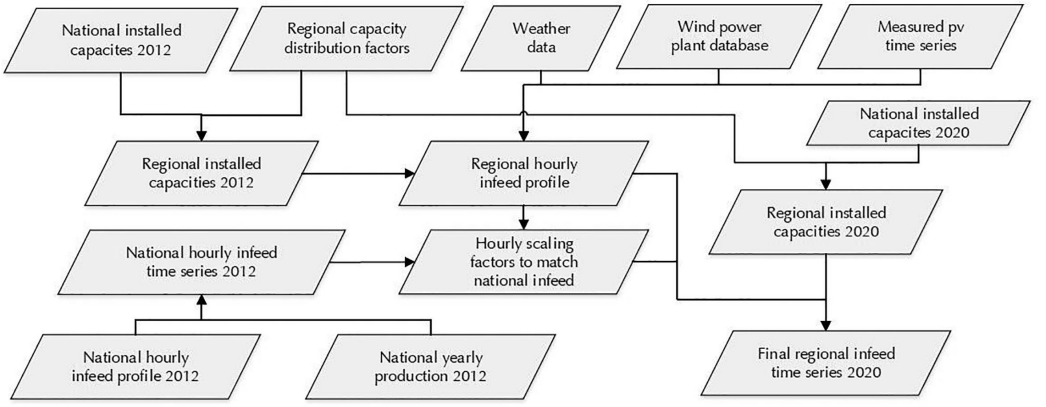

APPENDIX D. ADDITIONAL INFORMATION ON THE USED DATA

Table 6: Overview of the used data sources of the regional load and renewable models

data	source	comment
National load profiles for 2012	Entso-E (2015, 2016a)	
National yearly demand for 2012 and 2020	IEA,(2014)	Values from 2012 are assumed to be constant over time.
Load profiles for consumers < 100 MWh/year	Stromnetz Berlin (2013); MVV Netze (2013); Energienetze Offenbach (2013); EVNG (2013); Stadtwerke Landshut (2013)	Publications stem from German DSOs and are the basis for the profiles of households and the service sector.
Sector-wise regional GVA	Eurostat (2015b); Bundesamt für Statistik (2015)	
Regional inhabitants	Eurostat (2015)	
National renewable profiles for 2012	Open Power System Data (2019); Elia (2016)	For NL and LU, profiles from BE are used. For CH, the PV profile from DE and the wind profile from AT is used.
National yearly renewable production for 2012	IEA (2014) and individual research for offshore wind	
National renewable installed capacities for 2012	EurObserv'ER (2013a,b, 2014a,b) and individual research for offshore wind turbines	For PV and onshore wind, a linear increase within the is year is assumed. For offshore wind, discrete capacity changes as detected in the time series or by individual research are incorporated.
National renewable installed capacities for 2020	Entso-E (2015) and individual research for offshore wind turbines	A linear increase of capacity is assumed between given projections for January 2020 and January 2025.
Regional distribution factors for renewable capacity (i.e. usually regional installed capacities)	Statistik Austria (2013); VREG (2015); Elia (2015); 50Hertz et al. (2016); Ministère de la Transition Ecologique, (2015); Rijksoverheid (Government of the Netherlands) (2015); Eurostat, (2015a)	If for a country, only regional (yearly) production is available, it is transformed into capacities using the regional infeed profiles. If for a country the data resolution is only NUTS2 or NUTS1 level, the region's area is used for further distribution.
Weather data	Deutscher Wetterdienst (2017)	
Wind power plant data	The Wind Power (2014)	Including power curves and representative regional coordinates, hub heights and turbine types

Table 7: Yearly electricity consumption per country and sector including transmission losses and energy industries' own use in TWh

	AT	BE	CH	DE	FR	LU	NL
Overall	68.2	88.1	63.6	564.1	488.5	6.7	115.8
Residential	17.6	19.8	18.3	137.0	158.3	0.9	25.0
Industry and energy industry	29.0	39.4	18.4	239.9	132.3	3.0	39.0
Services, transport and others	17.9	24.8	22.2	162.6	163.7	2.6	47.2
Losses	3.7	4.1	4.6	24.6	34.3	0.1	4.5

Table 8: Costs per fuel (for all countries) in €MWh and CO_2 costs in €/t

Coal	Oil	Lignite	Natural gas	Nuclear	CO_2
7.92	29.00	1.51	21.74	1.01	8.15

Table 9: Range of variable costs of power plants per fuel and country in €/MWh

	AT	BE	CH	DE	FR	LU	NL
Biomass	1.4	1.4-1.5		1.5	1.3-1.5		1.4-1.5
Coal	28.0	26.6		25.1-31.0	27.6-50.7		26.9-28.0
Oil	72.3	66.2	66.4	65.1-107.2	61.7-109.1	66.4	62.9
Lignite				13.1-16.5			
Municipal waste	3.7	3.8	3.1-3.5	3.0-3.4	3.8	3.5	3.8
Natural gas	46.2-64.8	41.7-64.8	44.5-65.1	50.6-95.2	41.6-71.5	41.6	41.6-72.1
Nuclear		3.8	3.8	3.8	3.8		3.8

APPENDIX E. REDISPATCH SENSITIVITY

In Section 2.6.1, we have introduced the factor γ_u. Table 10 presents the corresponding redispatch amounts and costs for different γ_u values between 0 and 0.3. Results show that the amounts of redispatch do not vary significantly for different values of γ_u. The absolute difference between the maximum and minimum value is around 186 GWh, which corresponds to less than 1% of the redispatch amounts. Yet, regarding costs, there is a substantial difference. In absolute terms, RDC increase about 300 million € comparing the RDCs for $\gamma_u = 0$ and $\gamma_u = 0.3$. In relative terms, this constitutes an increase of about 21%.

Table 10: Sensitivity results for the factor γ_u in the BAU-C.

γ_u	0	0.1	0.2	0.3
pos. redispatch [TWh]	22.11	21.92	21.81	21.93
RDC [million EUR]	1,200	1,302	1,404	1,517
Δ RDC to $\gamma_u = 0.2$ [million EUR]	–204	–102	—	+113

Table 11 presents how the SC savings depend on the choice of γ_u for the different PZCs. We present the SC changes (ΔSC) calculated with the γ_u chosen in our case study (=0.2) and with the lower bound value ($\gamma_u = 0$). Thus, $\gamma_u = 0$ constitutes a worst-case approximation of the system cost savings. Obviously, RDCs calculated with $\gamma_u = 0$ are always lower than those calculated with $\gamma_u = 0.2$. In case of the 28-ImpC, the SC savings compared to the BAU-C would decrease from 948 million € to 744 million € (i.e. decreasing by 22%). Thus, one should be aware of the dependency on γ_u. However, the worst-case approximation yields savings of 744 million €, which still represents a very significant amount.

Table 11: Change in system costs ($SC_{X\text{–}ImpC}$–SC_{BAU}) calculated with $\gamma_u = 0.2$ and $\gamma_u = 0$.

PZC (x-ImpC with $\gamma_u = 0.2$)	5-ImpC	8-ImpC	14-ImpC	28-ImpC	50-ImpC
ΔSC for $\gamma_u = 0.2$	–0.76	–0.67	–0.71	–0.95	–0.57
ΔSC for $\gamma_u = 0$ in BAU-C	–0.56	–0.47	–0.51	–0.75	–0.37

APPENDIX F. NON-MONOTONIC RISE OF MARKET CLEARING COSTS

In Section 4.2/Figure 9, we have observed that MCC do not rise monotonically. This is non-intuitive, as one would expect MCC to rise with each added LFC. The intuition may be expressed formally by stating that, for any $f(\mathbf{q}) : \mathbb{R}^n \to \mathbb{R}$, $\min_{\mathbf{q}\in Q_1} f(\mathbf{q}) \geq \min_{\mathbf{q}\in Q_2} f(\mathbf{q})$ if $Q_1 \subset Q_2$. Therein, Q_1 and Q_2 are the sets of possible solutions, i.e. equivalent to the feasible region of the electricity market clearing problems (EMCPs) for PZC_1 and PZC_2. However, the expectation of

$Q_1 \subset Q_2$ represents a naive intuition. As a matter of fact, $Q_1 \subset Q_2$ is not necessarily the case if we consider PZC_1 to have more price zones than PZC_2. Basically, this can already be concluded from the analyses in Felten et al. (2021). In conjunction with the case study, the following three factors can yet be highlighted. For the explanation of these factors, we again consider a PZC_1 with more zones than PZC_2:

1. **Degrees of freedom:** Any additional PZ z increases the degrees of freedom of the EMCP. As shown in Felten et al. (2021), the choice of GSKs and of the base case defines a hyperplane through the nodal feasibility polyhedron. Thus, in this regard, the feasible region of the EMCP with more PZs tends to increase (i.e. influence towards $Q_1 \supset Q_2$). This is important for managing congestion on inter-zonal and intra-zonal lines (cf. Felten et al., 2021).
2. **Number of LFCs:** More LFCs tend to reduce the feasible region of the EMCP (i.e. influence towards $Q_1 \subset Q_2$).
3. **Inaccuracy of LFCs:** LFCs as defined in FBMC are subject to inaccuracies. I.e. they may be overly restrictive or too loose. This statement equally holds for LFCs of an EMCP with more or less price zones (cf. Felten et al., 2021). Therefore, no clear tendency towards an increasing or decreasing set of possible solutions is given a priori. However, this aspect may enhance the effect of additional LFCs being applied (item 2).[26]

All three points are observable in our case study. The effects under item 1 can be found at the transition from 14-ImpC to 28-ImpC. In 14-ImpC, the Northern German PZ 3 is dominated by wind generation. The most frequently binding LFC in the EMCP of 14-ImpC is the line "Sottrum-Blockland" presented in Figure 19. PZ 3 has a zonal PTDF value of approx. 0.259, which constitutes the highest line load sensitivity of all PZs on that line. In 28-ImpC, the PZ is split into two subzones. The new subzones 6 and 7 have the PTDFs 0.098 and 0.262 respectively. The split of PZ 3 (14-ImpC) into these two PZs yields one more degree of freedom in the EMCP. Thus, the EMCP considers that subzone 6 compounds much less to the congestion of this line than subzone 7. Therefore, the optimizer prefers infeed from subzone 6, and more wind energy can be integrated. In this region alone, approx. 0.6 TWh of additional wind energy is scheduled in the EMCP. Assuming the replacement of gas-based generation, this yields cost reductions of around 40 million . In order to show that the changed infeed has very little influence on line loadings, we plot a line overload histogram for the 4,861 time stamps where the LFC of line "Sottrum-Blockland" is binding in 14-ImpC (cf. Figure 20). Scheduled overloads are even reduced by approx. 22%, while integrating more wind generation.

The impact of more LFCs in the EMCP (cf. numeral 2) can be seen in 50-ImpC. In this configuration, PZ 13 has two major centers of generation capacities (cf. 50-ImpC in Figure 21). A large nuclear power plant is located in the north of PZ 13 surrounded by two coal-based power plants. Towards the eastern part of the zone, there is a lignite-based generation unit. And further towards the center of PZ13, there are 2 pumped storage power plants. PZ 13 has emerged from a

26. These inaccuracies may partly also be artefacts of the hierarchical cluster algorithm in conjunction with FBMC. Given its hierarchical structure, the identified solutions are close to optimal but not necessarily optimal PZCs with respect to the minimization of intrazonal LMP variation. [Felling and Weber(2018)] give an intuitive example on a 4-node network that underlines this context. Moreover, the PZCs are based on LMPs. I.e. FBMC-style LFCs are not taken into account in the cluster algorithm and, thus, optimality in a FBMC environment cannot be guaranteed. However, Entso-E's methods for endogenous PZCs determination [Entso-E(2018)] do not take into account FBMC-style LFCs either.

Figure 19: North DE: 14-ImpC PZ3 / 28-ImpC PZ 6 and PZ 7[27]

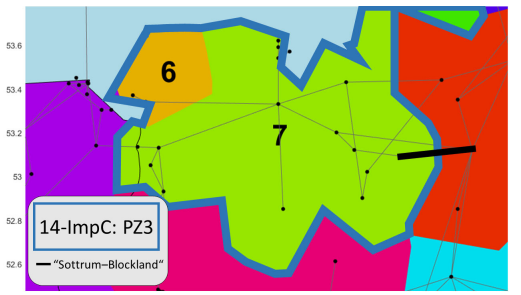

Figure 20: Overloads when binding in EMCP of 14-ImpC

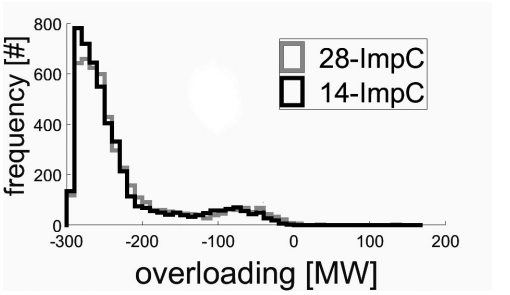

bigger zone (PZ 8 in 28-ImpC). Furthermore, its neighboring zones to the west, are also more fragmented than in 28-ImpC. Therefore, several new lines/LFCs are considered in the vicinity of PZ13 (cf. Figure 21).

Regarding the impact under numeral 3, the zonal PTDFs of PZ 13 are especially inaccurate for the lines in the east (connecting PZ 27 and PZ 29) and for the line parallel to its western delineation (connecting PZ 21 and PZ 25) in 50-ImpC. This is a consequence of using a weighted average of zonal PTDFs (cf. Felten et al. (2021). Thus, the line loads approximated by the FBMC approach are in particular inaccurate for the LFCs near PZ 13. This is seen in Figure 22. Therein, negative overloads are equivalent to underutilization of lines, i.e. LFCs are unnecessary restrictive. When the LFCs in the vicinity of PZ 13 are binding in 50-ImpC, actual line utilization is significantly below full usage. In sum, the line underutilization is 637 GWh. Exploiting these free line capacities would improve market outcomes without entailing redispatch. Using the FBMC approach, net exports from PZ 13 are seen to aggravate the load situation of these lines, and generation in PZ 13 is decreased—notably, decreased beyond what would be necessary. Therefore, only in PZ 13, PZ 27 and PZ 29, which had been one united zone in 28-ImpC, lignite-based generation decreases by around 2.4 TWh compared to 28-ImpC and coal-based generation decreases by around 1 TWh. This corresponds to MCC increases of around 180 million € (assuming substitution by gas-based generation).

Figure 21: DE East / West 50-ImpC[28]

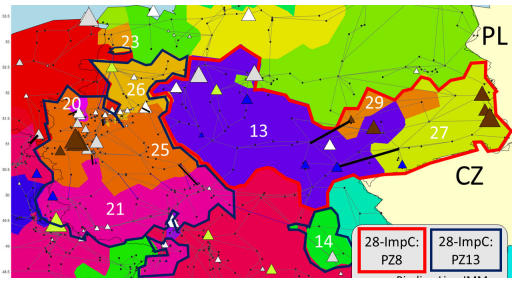

Figure 22: Overloads of lines close to PZ 13 (50-ImpC) when binding in EMCP.

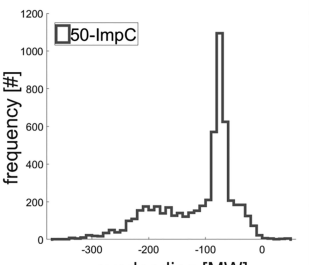

In conclusion, we have shown that monotonically rising MCC cannot be expected. This is a consequence of the inaccuracies inherent to FBMC procedures (cf. Felten et al. (2021) in combination with price zones derived by means of a hierarchical clustering algorithm. This result is quite

27. For colored illustrations please refer to the online version of the journal.
28. For colored illustrations please refer to the online version of the journal.

specific to FBMC and shows the importance of profound model-based assessments before deciding for a new PZC out of a variety of PZC options. Moreover, Felling (2019) and Ambrosius et al. (2020) come to similar conclusions that price zones based on LMPs may not be the optimal choice.

APPENDIX G. COMPUTATIONAL PERFORMANCE

Computation times for the JMM runs are presented in Table 12. The computation time depends strongly on the number of considered price zones, due to rising numbers of variables and constraints. Calculations were undertaken using an Intel Xeon E5-2637 v2 3,5 GHz CPU with 2 cores. However, as computation time was not the main focus of our study, we cannot exclude that other processes, that could have affected computational times, were run on the server at the same time.

Table 12: Approximative computation times of a market model run per configuration in hours

configuration	BAU-C	5	8	14	28	50
comp. time [h]	7.7	9.0	10.5	14.3	15.8	221.2

IAEE

International Association for
ENERGY ECONOMICS

Membership in the International Association for Energy Economics is open to anyone worldwide who has an interest in the fields of energy or energy economics. Our membership consists of those working in both the public and private sectors including government, academic and commercial. Our current member base consists of 3900+ members in over 110 nations, with 28 nations having local affiliate organization.

We are an independent, non-profit, global membership organization for business, government, academic and other professionals concerned with energy and related issues in the international community. We advance the knowledge, understanding and application of economics across all aspects of energy and foster communication amongst energy concerned professionals.

We are proud of our membership benefit offerings, which include access to a rich library of energy economics related publications and proceedings as well as a robust line-up of webinars, podcasts and conferences. Learn more about the benefits of membership at: https://www.iaee.org/en/membership/benefits.aspx

In addition to traditional membership, we offer student and institutional memberships.